Oceanologia, corrected, in press
Polish Academy of Sciences
Institute of Oceanology

https://doi.org/10.5697/NDCH3019

The effect of freshwater discharge on the microbial-induced precipitation of minerals in a Baltic Sea bottom pockmark

Grzegorz Rzepa[1,*], Andrzej Borkowski[1], Maciej Manecki[1], Aleksandra Brodecka-Goluch[2], Katarzyna Łukawska-Matuszewska[2], Jarosław Kania[1], Artur Błachowski[1], Paweł Działak[1], Izabela De Mey-Śnieżyńska[3]

Abstract
Seabed pockmarks are circular or elongated depressions usually formed by the outflow of methane and groundwater. The accumulation of organic matter and disruption of sediments by the seepage result in specific biogeochemical conditions affecting both porewater and sediment composition. In this study, we have shown how freshwater intrusions and the presence of methane affect the biogeochemistry and mineralogy of the pockmark environment within continental shelf sea sediments. Porewater and sediment samples collected during an active freshwater seepage were compared with samples taken from the same location between seeps and from a nearby reference station. Porewater chemistry and the mineralogy of the sediments were combined with thermodynamic modeling. The bacterial and archaeal taxa were also identified via metagenomic analysis. It was found that freshwater seepage modifies the composition of pore water and affects both the degree of supersaturation of solutions relative to sediment minerals and the composition of the microbial system. A conceptual model has been proposed indicating that changes in sediment mineral composition due to freshwater discharge reflect the response of the microbial community to changes in pore water composition.

Keywords
Marine sediments; Methane; Iron speciation; Authigenic minerals; Microbiology

[1]*Faculty of Geology, Geophysics and Environmental Protection, AGH University of Krakow, al. Mickiewicza 30, 30–059 Kraków, Poland*
[2]*Faculty of Oceanography and Geography, University of Gdańsk, al. Marszałka Piłsudskiego 46, 81–378 Gdynia, Poland*
[3]*Faculty of Geology, University of Warsaw, ul. Żwirki i Wigury 93, 02–089 Warsaw, Poland*
***Correspondence**: rzepa@agh.edu.pl (G. Rzepa)

Received: 5 May 2025; **revised:** 12 March 2026; **accepted**: 17 March 2026

Abbreviations

- AOM – anaerobic oxidation of methane.
- CMC – Ca-Mg carbonate.
- DIC – dissolved inorganic carbon.
- DOC – dissolved organic carbon.
- dSi – dissolved silica.
- FAAS – flame atomic absorption spectrophotometry.
- Fe_{CARB} – Fe in carbonates.
- Fe_{OX1} – Fe in 'labile' oxyhydroxides.
- Fe_{OX2} – Fe in 'crystalline' oxyhydroxides.
- Fe_{MAG} – Fe in magnetite.
- Fe_{S+PRS} – Fe in sulfides and poorly-reactive silicates.
- Fe_{TOT} – total Fe.
- FWHM – full width at half maximum.
- GC – gas chromatography.
- ICP-OES – inductively coupled plasma optical emission spectroscopy.
- IS – isomer shift.
- MS – Mössbauer spectroscopy.
- OM – organic matter.
- PCA – principal component analysis.

- PCoA – principal coordinate analysis.
- PW – porewater.
- QS – quadrupole splitting.
- RT – room temperature.
- SEM-EDS – scanning electron microscopy.
- SW – seawater.
- TDC – total dissolved carbon.
- XRD – X-ray diffractometry.

1. Introduction

Seabed pockmarks are found in oceans worldwide, mainly in estuaries and on the continental shelf (Hovland and Judd, 1988). They were first discovered in the second half of the 20th century during surveys on the continental shelf in the Atlantic Ocean off Canada (King and MacLean, 1970). Pockmarks are formed by the outflow of gas (usually biogenic methane) and groundwater from fine-grained unconsolidated sediments. The structures take the form of circular or elongated depressions at the bottom (Hovland and Judd, 1988; Hoffmann et al., 2020; Idczak et al., 2020). They vary greatly in size, with diameters ranging from a few centimeters to as much as 1 km and with depths up to 20–30 m (Scanlon and Knebel, 1985; Cole et al., 2000; Loncke and Mascle, 2004).

The presence of pockmarks and the associated gas or groundwater outflows affect the seabed morphology. Depressions in the bottom provide a natural sedimentation trap in which organic debris accumulates (Judd and Hovland, 2007; Idczak et al., 2020). The accumulation of organic matter (OM), combined with physical disruption of sediment by gas and groundwater seepage, results in specific biogeochemical conditions in pockmarks. Processes such as methanogenesis, anaerobic oxidation of methane (AOM), and dilution of pore waters by seeping groundwater make the chemical composition of pore waters in pockmarks significantly different from that of typical marine sediments (Pimenov et al., 2010; Hung et al., 2016; Idczak et al., 2020; Kurowski et al., 2024). This, in turn, may be reflected in the mineral composition of the sediment (Peckmann et al., 2001; Judd and Hovland, 2007), as the degree of saturation with specific mineral phases affects the possibility of precipitation (see, e.g., Walton, 1965; Suess, 1979; Burton, 1993). Among the minerals most actively precipitated in methane-bearing sediments are Mg-calcite and aragonite ($CaCO_3$), dolomite ($CaMg(CO_3)_2$), magnesite ($MgCO_3$), and Fe- and Mn-carbonates (Peckmann et al., 2001; Greinert et al., 2001; Teichert et al., 2005; Mavromatis et al., 2012; Łukawska-Matuszewska et al., 2022).

Microbiological studies show that pockmarks are hotspots of microbial biodiversity (Ruff et al., 2015). Prokaryote communities in sediments are shaped by freshwater seepage and bubbling methane, providing specialized environmental niches (Wegener et al., 2008; Haverkamp et al., 2014; Giovanelli et al., 2016). Specifically, increased prokaryotic abundance and biomass in the sediment (Giovanelli et al., 2016), a higher proportion of Archaea (Orcutt et al., 2005), and a higher abundance of methanotrophs and sulfide-oxidizing bacteria (Knittel et al., 2003; Ruff et al., 2015) are observed. Pockmark activity may also increase nutrient concentrations in the water column above pockmarks, further supporting biological productivity (Hovland and Judd, 1988; Zeppilli et al., 2012; O'Reilly et al., 2021). In the vicinity of the pockmarks, there is a greater quantity and diversity of benthic fauna and an increased concentration of seston, including phytoplankton (Webb et al., 2009).

Given the complexity of pockmarks and the variety of physical, chemical, geological, and biological processes, a multidisciplinary approach is required to study these structures. Chemical analysis of water or sediment alone is not sufficient to explain the mechanisms that lead to the specific mineral composition of the sediment or specific microbial diversity in pockmarks. Therefore, chemical studies of gas-bearing sediments and pore waters are more often combined with studies of the sediment mineralogy (Peckmann et al., 2001; Mavromatis et al., 2012; Kurowski et al., 2024) and microbiology (Idczak et al., 2020; O'Reilly et al., 2021; Iasakov et al., 2021; Brodecka-Goluch et al., 2022; Purkamo et al., 2022). However, this type of interdisciplinary research, covering mineralogical, geochemical, and microbiological aspects, is challenging and still rare, even though it allows for better understanding and detailed characterization of diagenetic processes in the sediment.

The present study was carried out in the Gulf of Gdańsk, located in the southern Baltic Sea. The occurrence of methane in the sediments of this area is documented by hydroacoustic investigations dating back to the 1990s (summarized by Jaśniewicz et al., 2019), showing various morphological structures related to the gas presence, i.e., pockmarks, gas-saturated sediments, and gas pockets. The Gulf of Gdańsk was also previously recognized as a region of freshwater seepage (Piekarek-Jankowska, 1994; Falkowska and Piekarek-Jankowska, 1999; Brodecka-Goluch et al., 2020; Szymczycha et al., 2023; Ehlert von Ahn et al., 2024). As the object of the present study, the MET1-BH pockmark was selected, which is unique compared to other structures found not only in the Gulf of Gdańsk (Matciak et al., 2024) but in the Baltic Sea in general (e.g. Whiticar and Werner, 1981; Söderberg and Flodén, 1997; Jakobsson et al., 2016; Virtasalo et al., 2019; Hoffmann et al., 2020). The MET1-BH pockmark represents a deep-water, below permanent halocline, site of groundwater

discharge, while most discharges in the Gulf of Gdańsk are located in shallower regions, mainly in the western part of the Gulf i.e. in Puck Bay (Szymczycha et al., 2023; Matciak et al., 2024). The freshwater flowing out of this pockmark has a distinct origin and chemical composition. In the outflows recorded in shallower areas, coastal drainage of shallow Holocene groundwater (Piekarek-Jankowska, 1994) or groundwater seeps mainly originating from Miocene–Pleistocene aquifers are observed (Dowgiałło and Kozerski, 1975; Matciak et al., 2024). In contrast, high concentrations of fluoride in the porewater of the MET1-BH pockmark (the so-called fluoride anomaly also observed in other parts of the region) indirectly indicate that groundwater originates from the Upper Cretaceous aquifer beneath the seafloor (Kozerski et al., 1987; Uścinowicz et al., 2011). This groundwater is of the HCO_3-Ca or HCO_3-Na type and exhibits a relatively high pH, up to 8.3 (Kozerski et al., 1987). The pockmark is relatively small (diameter of ~50 m) but much deeper (~9 m) compared to the extensive but shallow structures nearby at the same depth (~80 m). For example, the MET1-MP pockmark, less than 2 km away, is only about 2 m deep, but 1500 m long and 500 m wide (Idczak et al., 2020; Brodecka-Goluch et al., 2022). In contrast to these extensive structures characterized by scattered and rather small gas outflows from the seafloor (Majewski and Klusek, 2014), at the MET1-BH a constant methane release can be observed in the form of massive gas flares, even up to 70–80 m in height (Idczak et al., 2020). The freshwater outflow from the pockmark at the time of the research campaign was strong enough to reduce the salinity near the bottom to about 2, while the typical salinity in the deepwater part of the Gulf of Gdańsk, below the permanent halocline, is ca. 10–12 (Majewski, 1990). It can be expected that such a strong fluid outflow is crucial in shaping the biogeochemical conditions and mineral composition of sediment in the pockmark.

This work aimed to present the response of the pockmark bottom sediments to the perturbation caused by freshwater outflows. Changes were identified by comparing samples taken during freshwater discharge with those taken from the same location between freshwater outflows (1.5 years after the sampled seepage) and with samples taken at a reference station where freshwater outflows are not observed. Based on direct geochemical and microbiological analyses and mineralogical characterization of sediments taken from layers several centimeters below the bottom, a complex environmental response to freshwater outflow was found. A conceptual model of these processes has been proposed, indicating that freshwater discharge causes changes in mineral composition of the sediment that reflect the response of the microbial community to geochemical changes in pore water composition.

2. Material and methods

2.1 Sample collection

The samples were collected in the Gulf of Gdańsk (southern Baltic Sea) from stations MET1-BH and MET1-REF (Figure 1), during consecutive cruises onboard the r/v

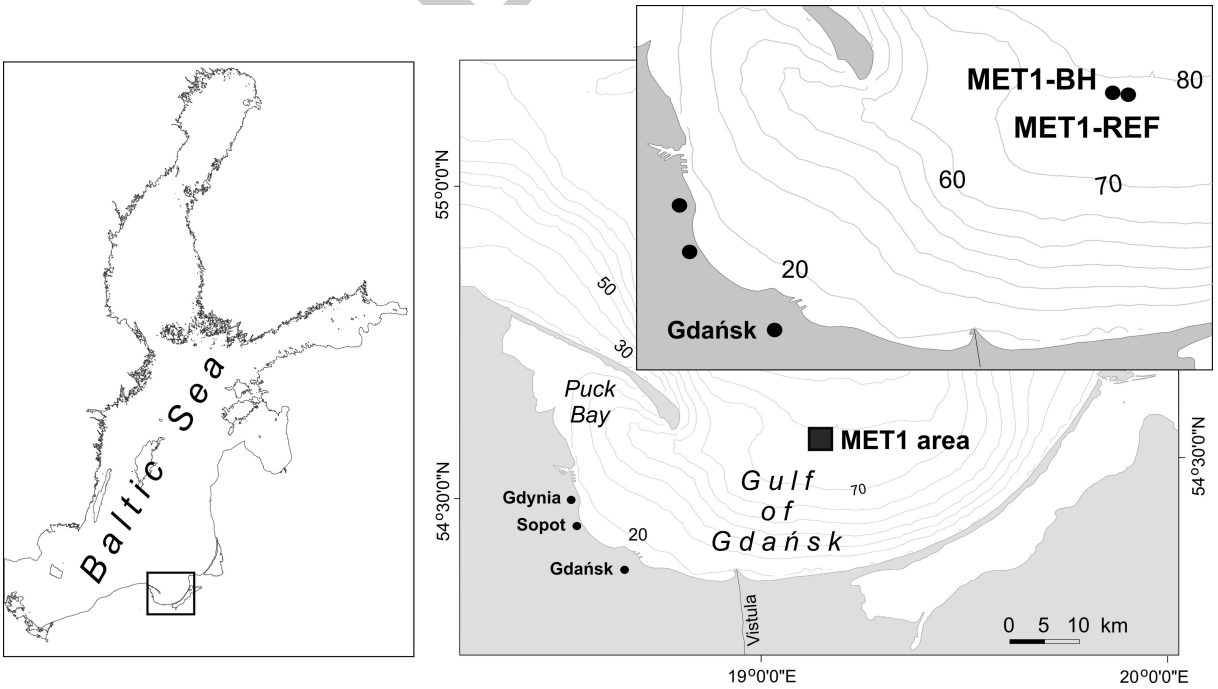

Figure 1. Map of the study area. The MET1-BH site was sampled during freshwater discharge (sample MET1-FRESH) and between discharges (sample MET1-SAL). The nearby MET1-REF location was sampled for reference.

Oceanograf (owned by the University of Gdańsk). The MET1-BH pockmark station was visited twice: in March 2019 during freshwater seepage (sample MET1-FRESH) and in February 2021 when no freshwater seepage was observed and a saline mass of water resided in the pockmark depression (sample MET1-SAL). Samples were also collected from the MET1-REF reference station, several hundred meters away. Sampling was always preceded by hydroacoustic measurements using EK80 split-beam echosounders (Simrad) and a sub-bottom profiler (Edge Tech SB-216S) to reproduce the exact sampling position (Figure S3). The precision of ship positioning and sediment sampling was achieved through the DP1 system. During sampling, r/v *Oceanograf* operated at sea in accordance with IHO S-44 measurement/survey standards (IHO S-44, 2020), where ship positioning and maintaining the position are strictly defined. Sediment samples were collected using Niemistö or Rumohr Lot gravity corers. Four sediment cores, 7.5 cm in diameter and approximately 100 cm long, were obtained at each station: one for mineralogical analyses and Fe speciation, two for pore waters and one for methane. The samples for microbiological analyses were collected only from MET1-REF and MET1-SAL (in the absence of freshwater) at depths of 10 cm, 50 cm, and 70–100 cm, depending on the core length.

The core for mineralogical analyses and Fe speciation was cut into 5-cm layers, using a PVC ring and a Teflon spatula. The layers were stored in polyethylene bags and frozen at −21°C until analysis. Fe forms were determined in every second layer. Mineralogical analyses were carried out in sediment layers taken from a depth of 5–10 cm bsf (below sea floor) in the MET1-FRESH core, 10–15 cm bsf in MET1-SAL, and 10–15 cm in MET1-REF. The pore water was retrieved from two cores at 5- or 10-cm intervals using Rhizon® samplers. The first sampler was placed 2–5 cm above the sediment-water interface (SWI) to collect near-bottom water. The obtained pore- and near-bottom water samples were analyzed for Na^+, K^+, Mg^{2+}, Ca^{2+}, Cl^-, Br^-, F^-, SO_4^{2-}, $\sum PO_4^{3-}$ (sum of PO_4^{3-}, HPO_4^{2-} and $H_2PO_4^-$), $\sum NH_4^+$ (sum of NH_4^+ and NH_3), $\sum H_2S$ (sum of H_2S, HS^- and S^{2-}), dissolved Si (dSi), Fe (Fe^{2+}) and Mn (Mn^{2+}) as well as total dissolved carbon (TDC), dissolved organic (DOC) and dissolved inorganic (DIC) carbon. The samples for methane analysis were taken directly from the Plexiglas core liners through 12-mm holes, using 3-ml syringes with the luer tip removed. The 2-ml samples were immediately transferred into 20-ml glass vials containing 2.5% NaOH, sealed with a butyl rubber stopper and an aluminum crimp cap (Jørgensen et al., 2001), shaken, and stored upside down at 4°C for GC analysis. Samples for microbial analysis were taken from MET1-SAL and MET1-REF cores using a sterile spatula and vials.

2.2 Geochemical analyses of sediments and pore waters

In pore- and near-bottom waters, the concentrations of Na, K, Mg, Ca, Fe, and Mn were analyzed using ICP-OES (Perkin-Elmer model OPTIMA 8300), while the concentrations of Cl^-, Br^-, F^- and SO_4^{2-} were determined using ion chromatography (DIONEX ICS1100/RFIC1600/20). Concentrations of $\sum NH_4^+$, $\sum PO_4^{3-}$, dSi, and $\sum H_2S$ were measured with spectrophotometric methods: $\sum NH_4^+$ by the indophenol blue method, $\sum PO_4^{3-}$ by the molybdenum blue method and $\sum H_2S$ using the methylene blue method (Grasshoff et al., 1999). The precision of the measurements (RSD) was 2.2%, 2.5%, and 2.0% for ammonia, phosphate and hydrogen sulfide, respectively. Concentrations of TDC, DIC, and DOC were measured in duplicates using high-temperature catalytic combustion and NDIR detection on the Vario TOC Cube (Elementar GmbH). DIC was separated from TDC by acidification of the sample with 1% H_3PO_4 inside the apparatus. TDC was determined by direct sample injection into the furnace while DIC was purged in the sparger and measured by the NDIR detector. DOC was determined as the difference between TDC and DIC. The accuracy (percentage of recovery) of DIC and DOC determination was 98% and 102%, respectively. Methane was analyzed using standard headspace techniques on a gas chromatograph (Perkin Elmer) equipped with a flame ionization detector FID and an HP-5 column (30 m, 0.32 mm, 0.25 μm). Helium was used as a carrier gas. The limit of detection was 0.2 $\mu mol/dm^3$. The results of methane determination were corrected for sediment porosity. Water content, loss on ignition, and porosity of the sediments are presented in the Supplementary Material (Figure S1, Table S1). Near-bottom and pore-water pH values were measured using a portable multimeter (WTW) and glass electrodes.

2.3 DNA isolation, sequencing, and data analyzing

Genomic DNA from the sediment samples was isolated using the EURx kit for complex matrix (Soil DNA Purification Kit, no E3570, EURX Ltd. Poland). The protocol requires mechanical homogenization of the samples to release cells from the sediment matrix. Isolated genomic DNA was subjected to metagenomic analysis (metabarcoding). Sequencing of the hypervariable V3-V4 region of the 16S rRNA gene was commissioned to GENOMED S.A. (Warsaw, Poland). Specific primer sequences (developed by Zymo Research, CA, USA) were used to amplify the selected region and prepare libraries (341F: CCTACGGGDGGCWGCAG, CCTAYGGGGYGCWGCAG, 806R: GACTACNVGGGTMTCTAATCC). PCR was performed using Q5 Hot Start High-Fidelity 2X Master Mix, with reaction conditions according to the manufacturer's recommendations. Sequencing was performed on a MiSeq sequencer, using the paired-end (PE) technology, 2x300nt, using Illumina's v3 kit. Fastq files were processed with fastp (0.23.2) (Chen et al., 2018) to improve the quality of raw sequences (cut-

ting adapters, filtering out bad quality reads, trimming, etc.). The sequences were further analyzed using Kraken2 (Wood et al., 2019) according to the protocol of the authors (Lu et al., 2022). The Silva database (v. 138) was used for taxonomic analysis (Quast et al., 2013). Then Bracken, set at the *Genus* level with a threshold set at 5, was applied to Kraken2 reports (Lu et al., 2017). The resulting data were transformed prior to analysis. To solve the problem of zero values, the results were imputed using the R package Compositions (v. 1.4.0.1) (Palarea-Albaladejo and Martín-Fernández, 2015). Then, the centered log-ratio transformation was applied to the data using the *Compositions* (v. 2.0-5) package for R (Aitchison, 1982; Quinn et al., 2019; Boogaart et al., 2023). Principal Coordinate Analysis (PCoA) was performed using the R package *stats* (v. 3.6.2) (R Core Team, 2022) and visualized using *ggplot2* (v. 3.4.2) (Wickham, 2009). Principal Component Analysis (PCA) was conducted using PCA from package FactoMineR, visualized with *factoextra* package. Pairwise plots of correlation matrices were performed using free Heatmapper software (Babicki et al., 2016). FAPROTAX (Functional Annotation of Prokaryotic Taxa) was used to establish functional community profiles and metabolic functions based on the bacterial and archaeal taxa identified in the samples (Louca et al., 2016).

2.4 Geochemical and mineralogical analysis of the sediment

The sediment for the determination of total Fe (Fe_{TOT}) and its fractionation was freeze-dried and homogenized to a fine powder in a ball mill with a porcelain vessel directly before analysis. Fe_{TOT} was determined after microwave digestion (approximately 0.25-0.30 g) with a mixture of trace metal grade concentrated HNO_3, HF, and HCl (v/v/v 1:2:1). The digested samples were diluted with 0.1 M HNO_3 (v/v 1:100) and Fe_{TOT} was measured by flame atomic absorption spectrophotometry (FAAS) using a Perkin Elmer AAnalyst 300. The analysis was carried out in triplicates. The precision of the determination was ≤5%. At the same time, Fe_{TOT} analysis in a certified reference material (BCR-320R) from the Institute for Reference Materials and Measurements was performed according to the same procedure. The recovery of Fe_{TOT} analysis from the certified material was 98%.

For Fe fractionation, the sequential extraction scheme by Poulton and Canfield (2005) was applied. An aliquot of approximately 0.1 g of sediment was placed in a plastic tube and a sequential four-stage extraction was performed: 1 M Na-acetate (pH = 4.5) for Fe carbonates (Fe_{CARB}); 1 M hydroxylamine-HCl (pH < 2) for labile Fe oxyhydroxides, i.e. ferrihydrite and lepidocrocite (Fe_{OX1}); 0.3 M Na-dithionite (pH = 4.8) for crystalline Fe (oxyhydr)oxides such as goethite, hematite, and akaganéite (Fe_{OX2}); and 0.2 M ammonium oxalate (pH = 3.2) for magnetite (Fe_{MAG}). The extracts were diluted (v/v 1:10) with 0.1 M HNO_3 and analyzed by FAAS. The difference between total iron (Fe_{TOT}) and the four extracted forms of Fe is the sum of iron bound to poorly reactive sheet silicates and iron in sulfides (Fe_{S+PRS}).

The mineral composition of the sediments was evaluated using powder X-ray diffractometry (XRD), scanning electron microscopy (SEM-EDS), and Mössbauer spectroscopy (MS). XRD patterns were collected using a Rigaku SmartLab instrument equipped with a graphite monochromator and rotation Cu anode, 45 kV and 200 mA generator settings, a 2–75° 2Θ recording range, a 0.05° step size, and a counting time of 1 second per step. Before analysis, the samples were gently ground using agate mortar covered with 96% ethanol. The samples, in the form of a paste, were then placed on a quartz plate and covered with plastic foil to prevent oxidation. The XRD patterns were evaluated using the diffraction pattern database of the International Centre for Diffraction Data. SEM analyses were conducted in low-vacuum mode using a FEI 200 Quanta FEG microscope equipped with an EDS/EDAX spectrometer. Acceleration voltage and pressure were 15–20 kV and 60 Pa, respectively. The samples were not coated with a conductive layer. ^{57}Fe Mössbauer spectroscopy measurements were performed in transmission geometry applying the RENON MsAa-4 (Błachowski et al., 2008) spectrometer operated in the round-corner triangular mode and equipped with the LND Kr-filled proportional detector. The He-Ne laser-based interferometer was used to calibrate a velocity scale. A single-line commercial ^{57}Co(Rh) source was kept at room temperature. An integral transmission approximation was applied to fit Mössbauer spectra using the MOSGRAF data processing software suite. Spectral isomer shifts (IS) are reported relative to the isomer (center) shift of room-temperature α-Fe. The absorbers for Mössbauer measurements were prepared using 45 mg/cm^2 of the investigated materials. The measurements were performed at room temperature and at 80 K to determine the possible presence of superparamagnetic nanoparticles of iron (oxyhydr)oxides. The SVT-400 cryostat by Janis Research Inc. was used to maintain the absorber temperature.

The thermodynamic equilibrium state of the studied waters and the mineral-water interaction was modeled using the PHREEQCI program (version 3.6) accompanied by the validated thermodynamic database (Parkhust and Appelo, 2013). Speciation of the solutions and saturation indices of selected minerals were compared for the water overlying the bottom and for pore waters both in the pockmark (when the freshwater seepage was not observed and during the seepage) as well as at the reference station.

3. Results

3.1 Geochemistry of pore water

Pore water chemistry is presented in Figures 2 and 3. Analysis revealed freshwater input at MET1-FRESH, where the salinity above the sediment was around 2, indicating a low-

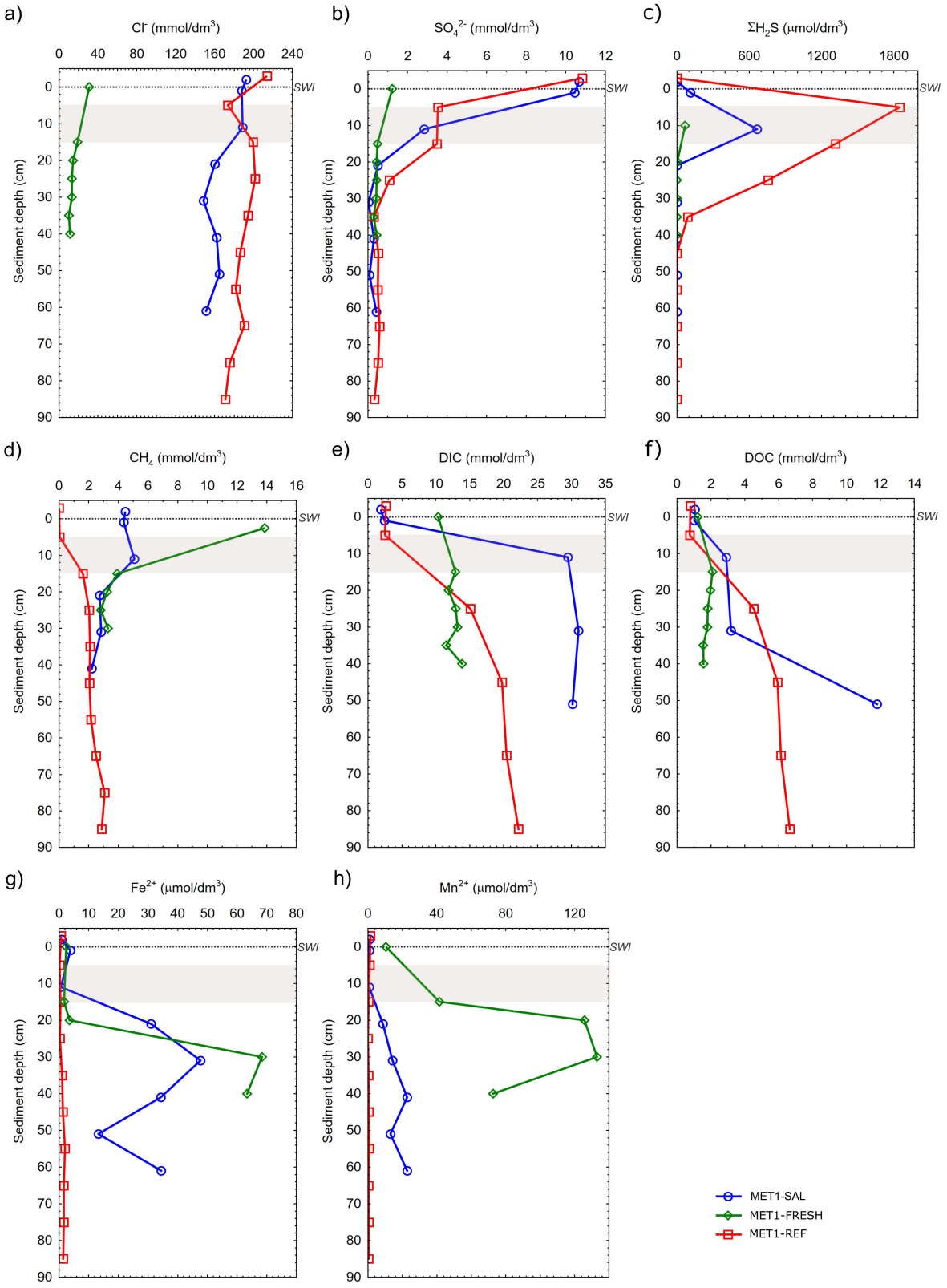

Figure 2. Concentrations of chloride (Cl^-) (a), sulfate (SO_4^{2-}) (b), hydrogen sulfide ($\sum H_2S$) (c), methane (CH_4) (d), dissolved inorganic carbon (DIC) (e), dissolved organic carbon (DOC)(f), dissolved iron (Fe^{2+}) (g), and manganese (Mn^{2+}) (h) in bottom and pore water at three research stations. SWI stands for sediment-water interface. Sediments for mineralogical analyses were collected at the depth denoted by gray bars.

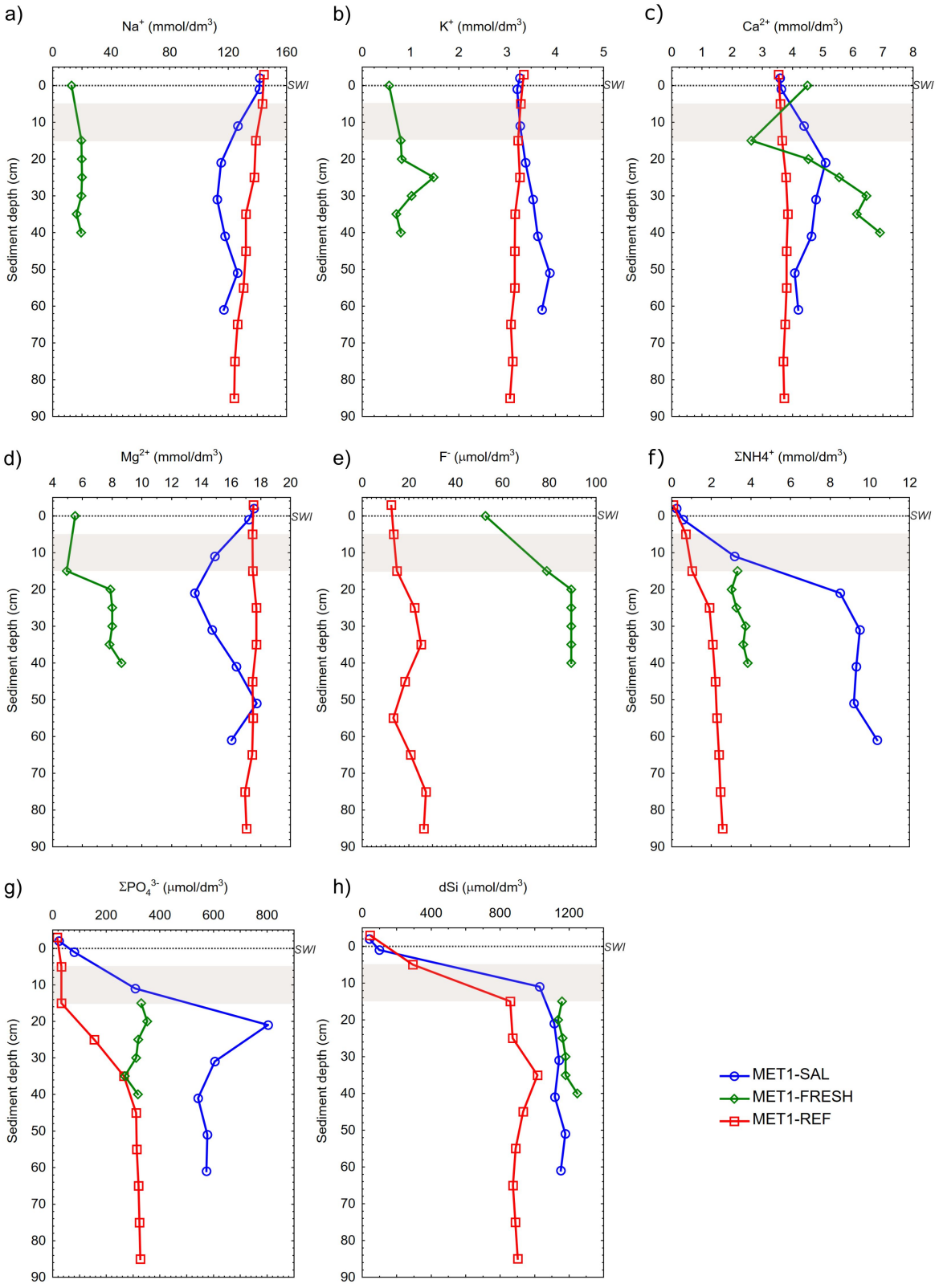

Figure 3. Concentrations of major cations (Na^+ – sodium, K^+ – potassium, Ca^{2+} – calcium, Mg^{2+} – magnesium) (a–d), fluoride (F^-) (e), ammonia ($\sum NH^{4+}$) (f), phosphate ($\sum PO_4^{3-}$) (g) and silicate (dSi) (h) in bottom and pore water at three research stations. SWI stands for sediment-water interface. Sediments for mineralogical analyses were collected at the depth denoted by grey bars.

salinity environment. As a result of freshwater seepage, Cl^- concentrations at MET1-FRESH were reduced below 19 mmol/dm^3 (Figure 2a) and were one order of magnitude lower compared to the values associated with typical salinity in the water column in the area (e.g., 150–200 mmol/dm^3; Łukawska-Matuszewska, 2016). On the contrary, the Cl^- content of the pore water at MET1-SAL was several times higher than that at MET1-FRESH, and comparable to the MET1-REF reference station (Figure 2a). While Cl^- concentrations near the sediment surface were similar to those in bottom water, a minor decline deeper in the profile suggested some fresh groundwater influence, although these values remained significantly higher than at MET1-FRESH. The salinity at MET1-SAL was about 9.6, comparable to the reference site (approximately 10.0), indicating that any potential freshwater intrusion was much less significant than during the MET1-FRESH scenario.

The concentrations of major cations (Na^+, K^+, Mg^{2+}) measured at MET1-FRESH were also significantly lower compared to the values recorded in the other two samples (Figure 3a,b,d). The opposite occurred for F^- (Figure 3e), the concentrations of which during freshwater seepage were several times higher (average 82.7 µmol/dm^3) compared to those at the reference station (average 19.4 µmol/dm^3).

Freshwater seeping from deeper layers also contributed to low pore water sulfate concentrations at MET1-FRESH, which did not exceed 0.49 mmol/dm^3 (Figure 2b). In comparison, the maximum concentration of SO_4^{2-} at MET1-REF and MET1-SAL was 3.53 mmol/dm^3 and 10.43 mmol/dm^3, respectively. As a result of lower sulfate availability and limited microbial sulfate reduction, hydrogen sulfide concentrations in MET1-FRESH pore waters (maximum $\sum H_2S = 66$ µmol/dm^3) were up to two orders of magnitude lower than in MET1-SAL or MET1-REF (663 µmol/dm^3 and 1850 µmol/dm^3, respectively) (Figure 2c).

The MET1-FRESH pockmark sediments contained more methane (Figure 2d). The concentration of methane reached 13.9 mmol/dm^3 at MET1-FRESH, while at MET1-SAL and MET1-REF, it did not exceed 5.1 and 3.1 mmol/dm^3, respectively. For MET1-FRESH, the concentration of CH_4 increased abruptly in the surface sediment layer, where it was nearly four times higher than in the layers below. At MET1-REF station, there was a gradual increase in CH_4 concentration, reaching a maximum value at 75 cm below the sediment surface.

During freshwater seepage, the concentration of DIC and DOC was at a near-constant level throughout the sediment profile (Figure 2e,f). In the other two profiles, the concentration of both forms increased with sediment depth. The concentration of DIC in the upper 10 cm of the pockmark sediment was significantly higher than at the reference station, regardless of freshwater outflow (Figure 2e).

Concentrations of Fe and Mn at MET1-FRESH and MET1-SAL were higher than at the reference station (Figure 2g,h). During the discharge, concentrations of these ions increased significantly up to 68 µmol Fe/dm^3 and 133 µmol Mn/dm^3, indicating more intensive participation of Fe(III) and Mn(IV) in oxidation processes.

In general, the pockmark sediments revealed higher concentrations of phosphate, ammonia, and silicate compared to those at the reference station (Figure 3f,g,h). At the reference station, the concentration of $\sum PO_4^{3-}$ did not exceed 327 µmol/dm^3, whereas in the pockmark it reached 803 µmol/dm^3 (Figure 3g). Also, the concentration of NH_4^+ at the reference station (708–2570 µmol/dm^3) was lower than at the pockmark, where, except for the surface sediment layer at MET-SAL, it was higher than 3000 µmol/dm^3 (Figure 3f).

3.2 Microbiology of the system

3.2.1 Microbial communities

The composition of the bacterial communities differed depending on the location and the sediment depth (Figure 4a). The most important bacterial classes in all samples were Gammaproteobacteria, Desulfobacteria, Cyanobacteriia, Clostridia, Bacteroidiia and Bacilli as well as Anaerolineae and Alphaproteobacteria. Virtually all classes were present in all samples, but the relative ratios between the classes were different (Figure 4a). For example, samples MET1-SAL (at all depths) and MET1-REF (at 10 cm) were similar in terms of relative abundance of Bacilli, Bacteroidiia or Gammaproteobacteria. However, samples MET1-REF at 50 cm and 1.0 m were different. The same was true in the case of the archaeal community composition (Figure 4b). However, the differences were more visible here. In particular, the 10 cm MET1-REF sample appeared to be noticeably different from other samples, e.g., due to the high relative abundance of class Nanoarchaeia, where members of ordo Woesearchaeales were noted. The MET1-REF samples from 50 cm and 1.0 m were characterized by the highest relative content of the Nitrososphaeria class. Differences found in the composition of the microbial community should be reflected in the grouping of the samples and indicate their distinctiveness from each other. This, in turn, should indicate that the studied sites are significantly different for some reason. Indeed, Principal Coordinate Analysis (PCoA) showed that all MET1-SAL samples are located close to each other in the Euclidean space, while the two deep MET1-REF samples form a separate group. The surface MET1-REF sample (10 cm) is also located separately (Figure 4c). The differences were consistent with those shown in the bar charts. There is another way to check whether the samples tested are different. If the samples come from microbiologically similar niches, then their microbial compositions should correlate to some extent. That is, the relative proportions of different groups of microorganisms should be similar. A correlation matrix between samples (Figure 4d) showed that the MET1-REF samples from 50 cm and 1.0 m depth

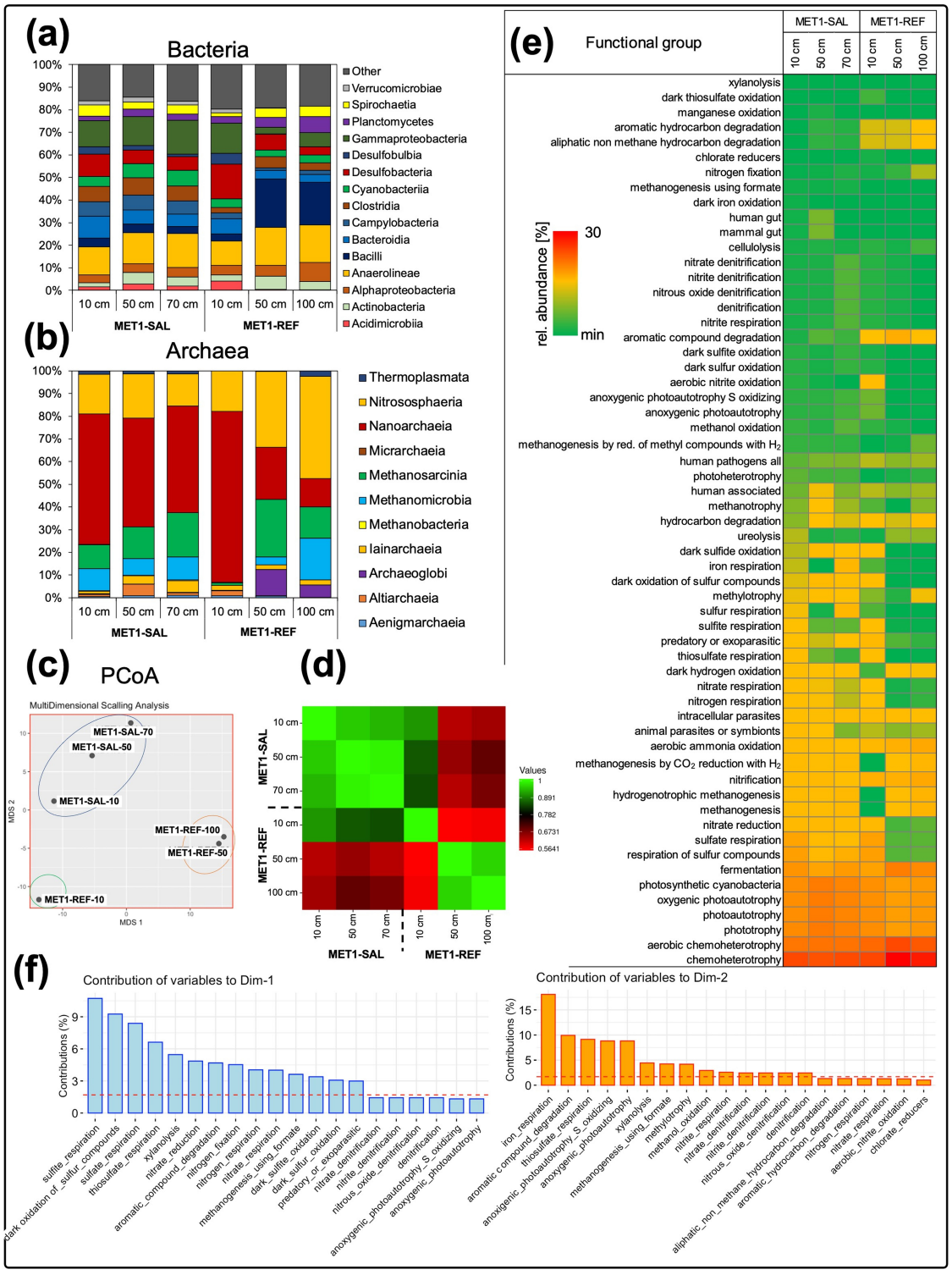

Figure 4. Metabarcoding 16S rDNA analysis. Bar plot of bacterial community composition (a) and archaeal community compositions (b) at class level. Principal Coordinate Analysis of microbial community at class level for samples (c) (based on the structure of bacterial and archaeal communities). Pairwise correlation matrix for samples (d). Functional community profiles and metabolic functions based on the microbial taxa (bacterial and archaeal) identified in the samples (e). Contribution of variables (functional groups) to dimension 1 and dimension 2 of Principal Component Analysis showing the most important groups differentiating the samples (f). A reference dashed line is shown. Column with a contribution above the reference line can be considered as important in contributing to the dimension (a function included in the FactoMineR package).

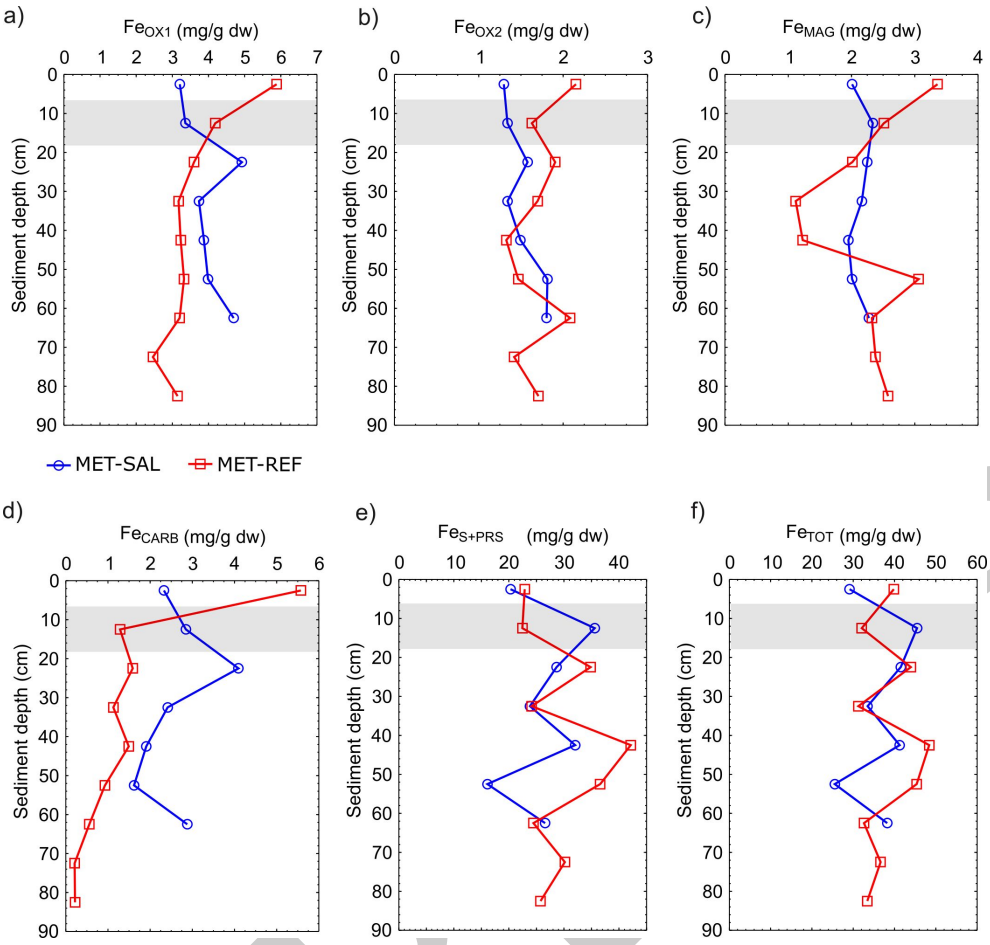

Figure 5. Concentration of iron in labile oxyhydroxides (Fe_{OX1}) (a), iron in crystalline oxyhydroxides (Fe_{OX2}) (b), iron in magnetite (Fe_{MAG}) (c), iron in carbonates (Fe_{CARB}) (d), iron in sulfides and poorly reactive silicate sheets (Fe_{S+PRS}) (e), and total iron (Fe_{TOT}) (f) in sediments of the pockmark MET1-SAL and reference station MET1-REF. Sediments for mineralogical analyses were collected at the depth denoted by gray bars.

did not correlate with the other samples. In contrast, the MET1-REF 10 cm sample showed a weaker correlation with the MET1-SAL samples. All samples from MET1-BH are significantly correlated with each other in terms of microbial community composition. These results indicate that the conditions are quite similar throughout the pockmark profile. In contrast, the conditions and hence microbial composition vary with depth in the reference site (MET1-REF).

3.2.2 Functional community profiles

Based on the identified bacterial and archaeal taxa, potential functional profiles could be established (Figure 4e). It should be noted here that this approach was not based on analyses of the presence of enzyme genes of specific processes. Only the potential physiological characteristics of the groups of microorganisms found in the samples were analyzed. Therefore, the functional profiles obtained were only an approximation of the metabolic potential of the microbial communities present in the samples. The analysis showed that the MET1-REF samples from 50 cm and 1.0 m were functionally different from the other samples. This was particularly evident for sulfur metabolism (sulfide oxidation, sulfur and sulfite respiration, and sulfate respiration). Similar differences were found for nitrogen metabolism (aerobic nitrite oxidation, nitrate respiration, nitrogen respiration, and nitrate reduction) and iron. In terms of methane metabolism, all the pockmark samples showed potential for methanogenesis, while the surface sample from MET1-REF (10 cm) showed no such feature. Only the deeper samples from MET1-REF, where sulfate influx is presumably reduced, showed a higher methanogenic potential. On the other hand, the overall functional potential toward chemoheterotrophy was similar in all samples regardless of the site. However, there were differences in the metabolism of aliphatic and aromatic hydrocarbons. PCA analysis allowed for the separation of those groups that have the greatest contribution to the variability of the samples (Figure 4f). It turns out that the groups respon-

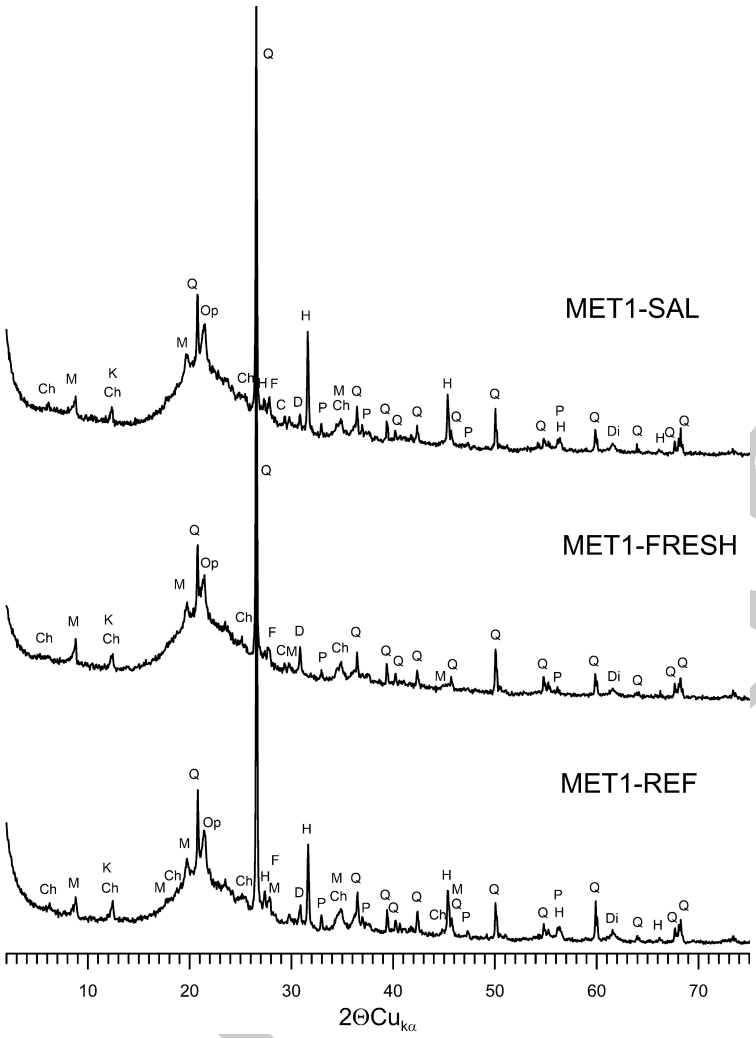

Figure 6. Mineral composition of the sediments determined by XRD. Q – quartz, Op – opal, M – 10 Å mica-type mineral(s), Ch – chlorite, K – kaolinite, H – halite, P – pyrite, D – CMC carbonate, C – calcite, F – feldspar, Di – *(060)* peak of dioctahedral phyllosilicates. Halite precipitated from pore water upon drying. The elevated background around 20° 2Θ indicates the presence of amorphous substances.

sible for the metabolism of sulfur, and iron, and groups conducting hydrocarbon degradation processes can differentiate the samples the most. The activity of microorganisms conducting the above-mentioned processes can lead to local differentiation of the environmental chemistry and, consequently, affect the precipitation of mineral phases.

3.3 Mineralogy and geochemistry of sediments

3.3.1 Iron fractionation

The contents of Fe_{TOT} and Fe forms are shown in Figure 5. Fe_{TOT} ranged from 25.5 to 48.4 mg/g dw (dry weight), with similar average values at MET1-SAL and MET1-REF station (36.4 mg/g dw and 38.2 mg/g, respectively) and irregular variation with depth (Figure 5f). While the concentrations of Fe_{TOT} and Fe_{S+PRS} (Fe in sulfides and poorly reactive silicates) of both stations were similar, the stations differed in other forms of Fe. This was particularly evident for Fe bound in carbonates (Fe_{CARB}). The sediment in the pockmark was enriched in Fe_{CARB} compared to the reference station (Figure 5d). The average Fe_{CARB} concentration in the pockmark was 2.6 mg/g dw, while at the reference station, it was 1.4 mg/g dw. At the pockmark, variations in Fe_{CARB} with depth were irregular, while there was a gradual decrease of this Fe form at the reference station.

MET1-SAL and MET1-REF were similar in terms of the content of Fe (oxyhydr)oxides (Fe_{OX1}, Fe_{OX2}, and Fe_{MAG} forms) in the sediment. At MET1-SAL, the average content of Fe_{OX1} was 3.8 ± 0.6 mg/g dw, Fe_{OX2} was 1.5 ± 0.2 mg/g dw, and Fe_{MAG} was 2.1 ± 0.2 mg/g dw. The concentration of the same Fe forms in the sediment at the MET1-REF station was 3.6 ± 1.0 mg/g dw, 1.7 ± 0.3 mg/g dw, and Fe_{MAG}

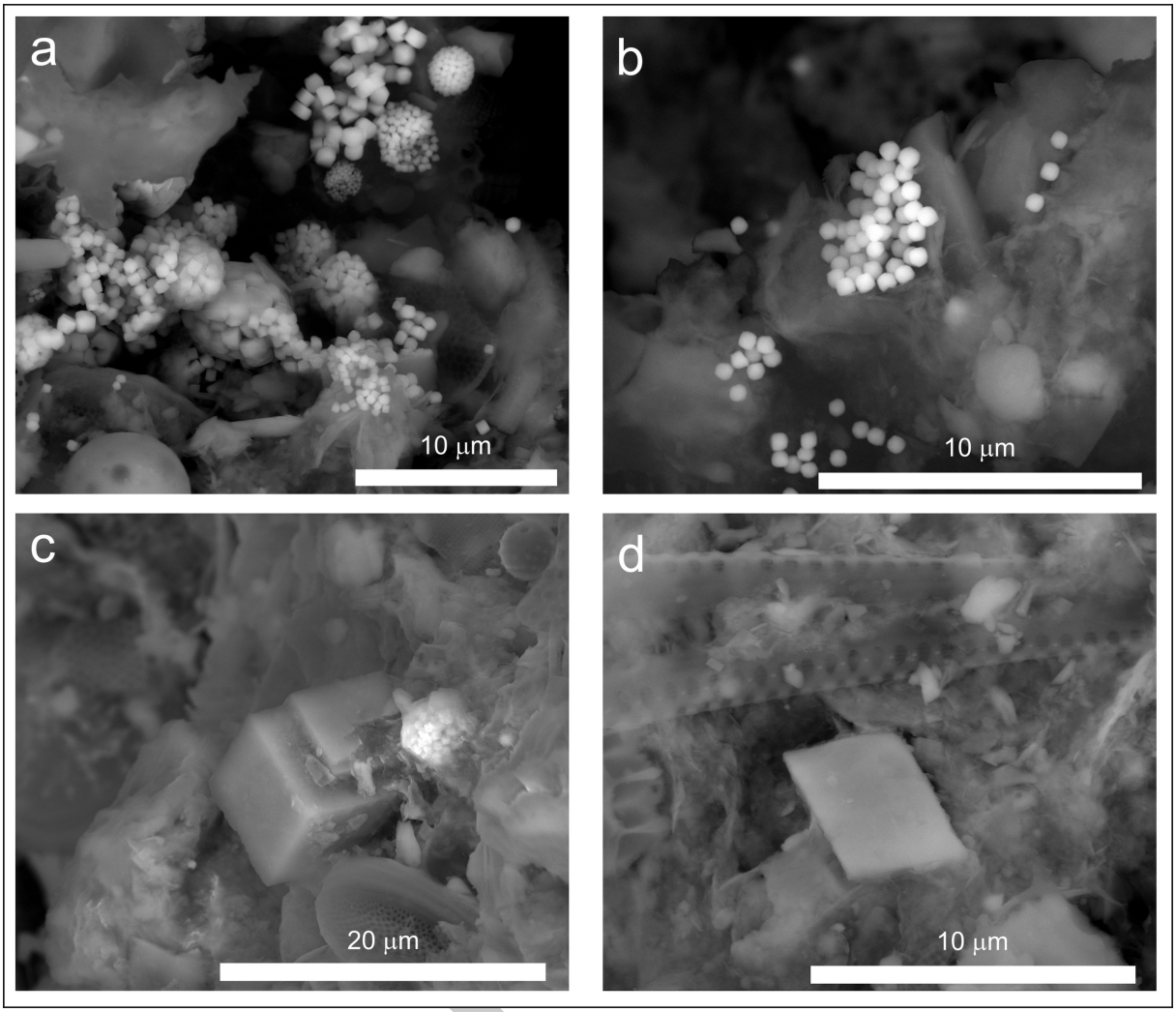

Figure 7. SEM images of the sediments. Various forms of pyrite accumulations in MET1-REF (a), disseminated pyrite crystals in MET1-SAL (b), euhedral CMC and small framboidal pyrite in MET1-FRESH (c), euhedral CMC in MET1-REF (d).

was 2.3 ± 0.8 mg/g dw, respectively. The content of all these three forms of Fe was more uniform in the sediment profile of the pockmark (Figure 5a,b,c). At the MET1-REF station, the surface layer of sediment contained more Fe (oxyhydr)oxides compared to the deeper sediment layers, which was particularly evident in the upper 15 cm of the sediment.

3.3.2 Mineralogical analyses

All sediments were fine-grained and dominated by (alumino)silicates. They were chiefly phyllosilicates, represented – according to the XRD patterns – by mica/illite, chlorite, and probably kaolinite. A *(060)* reflection positioned at ca. 1.50 Å (Figure 6) suggests that the phyllosilicates are predominately dioctahedral (Moore and Reynolds, 1997). Silica polymorphs were also abundant, including detrital quartz and authigenic opal-type silica with variable degrees of structural order. Feldspars were frequently encountered and involved mainly potassium feldspars while sodium-rich plagioclases were less common. All the silicate components mentioned above were present in the studied sediments in similar amounts and proportions.

The differences between the sediments were apparent when the presence and amount of authigenic accessory minerals, mainly sulfides and carbonates, were compared. Ferric disulfide – pyrite was present in all the samples. It was, however, more abundant in the reference station (MET1-REF) where raspberry-like framboidal accumulations with a diameter of up to some 20 μm were encountered (Figure 7a). Small isometric, usually cubic pyrite crystals were also dispersed within the sediment here (Figure 7b). On the contrary, in the pockmark sediments (MET1-SAL and MET1-FRESH), pyrite was less abundant and occurred more often in a dispersed form, whereas

Table 1. ^{57}Fe Mössbauer spectroscopy parameters. A – relative area of respective spectral component corresponding (with some approximation) to relative contribution of Fe atoms into respective iron phase, IS – isomer (center) shift relative to α-Fe at RT, QS – quadrupole splitting, Γ – spectral line-width (full width at half maximum FWHM). Errors are of the order of unity for the last digit shown.

Sample	Iron valence state	A [%]	IS [mm/s]	QS [mm/s]	Γ [mm/s]
MET1-FRESH	Fe^{2+} (pyrite)	63	0.32	0.61	0.46
5–10 cm	Fe^{2+} (silicate-1)	22	1.13	2.61	0.35
RT	Fe^{2+} (silicate-2)	9	1.18	1.97	0.50
	Fe^{3+}	6	0.33	1.23	0.36
MET1-FRESH	Fe^{2+} (pyrite)	59	0.44	0.59	0.43
5–10 cm	Fe^{2+} (silicate-1)	16	1.26	2.95	0.28
80 K	Fe^{2+} (silicate-2)	13	1.27	2.59	0.34
	Fe^{3+}	12	0.44	1.15	0.38
MET1-SAL	Fe^{2+} (pyrite)	62	0.43	0.59	0.42
10–15 cm	Fe^{2+} (silicate-1)	17	1.26	2.95	0.29
80 K	Fe^{2+} (silicate-2)	12	1.27	2.59	0.38
	Fe^{3+}	9	0.44	1.17	0.39
MET1-REF	Fe^{2+} (pyrite)	64	0.31	0.62	0.37
RT	Fe^{2+} (silicate-1)	17	1.14	2.67	0.28
	Fe^{2+} (silicate-2)	14	1.22	2.18	0.49
	Fe^{3+}	5	0.34	1.24	0.33
MET1-REF	Fe^{2+} (pyrite)	64	0.42	0.59	0.41
80 K	Fe^{2+} (silicate-1)	14	1.24	2.92	0.29
	Fe^{2+} (silicate-2)	17	1.24	2.64	0.36
	Fe^{3+}	5	0.42	1.18	0.32

framboids were encountered sporadically (Figure 7c). This was also reflected in the X-ray diffraction patterns, where the peaks attributable to pyrite were more intense in the case of MET1-REF (Figure 6).

All the studied sediment samples contained accessory carbonates, mainly a Ca-Mg carbonate (CMC: high-Mg calcite and/or dolomite – $CaMg(CO_3)_2$). It was much more common in the sediment from the pockmark (MET1-FRESH and MET1-SAL) where euhedral crystals up to 15–20 μm in size were relatively often observed (Figure 7c,d). This was consistent with the peak around 2.88 Å in XRD patterns, usually attributed to dolomite (Figure 6). There was much less CMC at MET1-REF as only sporadic euhedral crystals were found (Figure 7). The content of CMC in the sediment is so low that limitations of X-ray diffraction make an unambiguous interpretation impossible. The reflections from planes with Miller indices *(101)*, *(015)*, and *(021)*, which are indicative of Ca-Mg ordering and the R $\overline{3}$ space group of dolomite (Gregg et al., 2015), are not apparent. On the other hand, micro-area EDS analysis of euhedral crystals revealed approximately equal Ca and Mg molar proportions. The carbonate always contained a small Fe admixture and traces of Mn, but probably too small to affect the position of the *(104)* peak. Also, Mössbauer spectroscopy indicates the lack of significant Fe substitution in CMC. Although according to these observations the presence of authigenic dolomite cannot be excluded, a further confirmation of Ca-Mg ordering in the carbonate is required. The appearance of a peak of 3.03 Åin the XRD patterns of both samples from the pockmark (Figure 6) indicated the presence of trace amounts of calcite ($CaCO_3$). This peak was absent in the sediment from the reference station.

^{57}Fe Mössbauer spectra are shown in Figure 8 and the spectral parameters are summarized in Table 1. All the spectra were similar (Figure 8). The main component of the spectra was a doublet with quadrupole splitting QS ~0.6 mm/s and isomer shift IS ~0.3 mm/s (at RT) characteristic of low-spin Fe^{2+} in pyrite (Dyar et al., 2006; Byrne and Kappler, 2019). The area of this subspectrum indicates that about 60% or more of the iron atoms were located in this sulfide. Although the contents of pyrite are similar, the area of the pyrite subspectrum is slightly higher in MET1-REF compared to MET1-FRESH and MET1-BH (Table 1), which is in good agreement with XRD analysis and SEM imaging. Another spectral component with a contribution of about 30% was two doublets with the hyperfine parameters characteristic of high-spin Fe^{2+} probably in (alumino)silicates like chlorite or illite (Dyar et al., 2006). A minor spectral component with an area of about 5–12% was a doublet typical for high-spin Fe^{3+}. The small area of this subspectrum made it difficult to reliably assign it to a specific iron phase. The results of ^{57}Fe Mössbauer spectroscopy indicate that about 90% of Fe atoms in the studied sediments were divalent which results from the strong reducing and anoxic conditions prevailing in this environment. The spectra did not contain sextets characteristic of magnetic iron (oxyhydr)oxides.

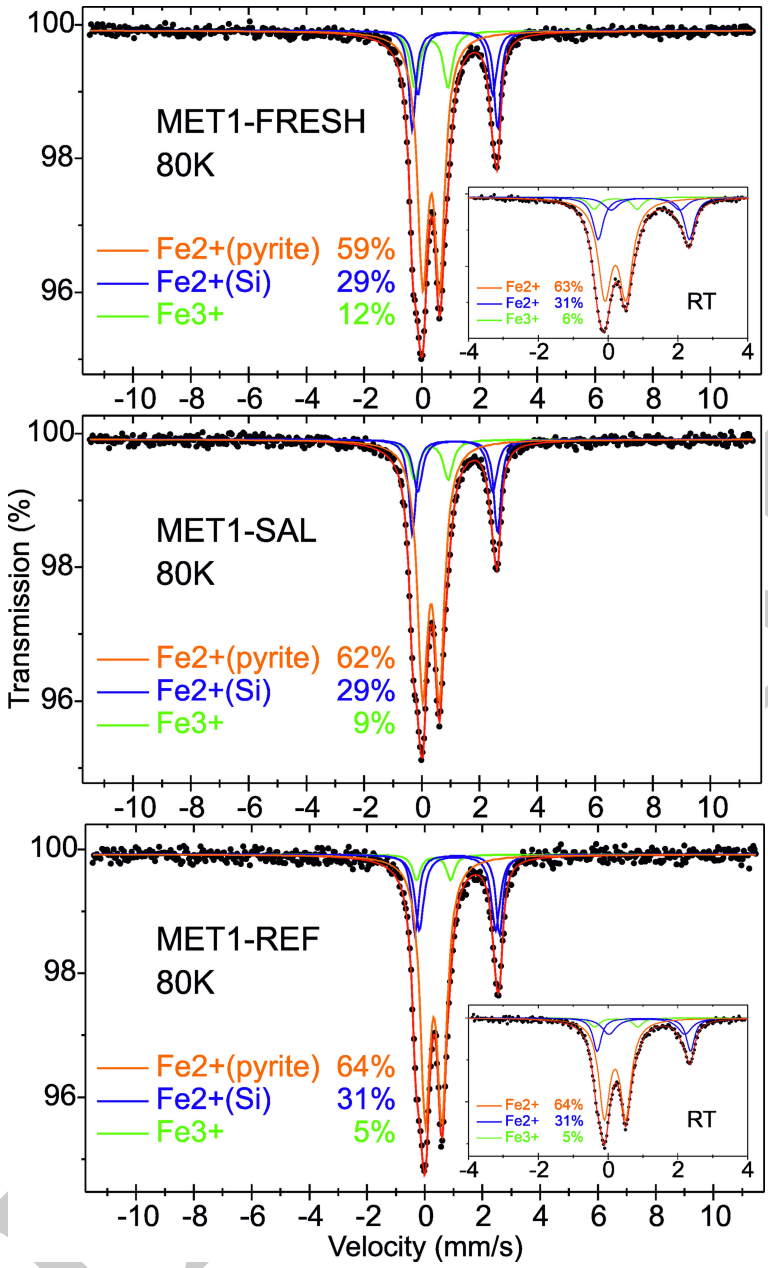

Figure 8. ^{57}Fe Mössbauer spectra of samples measured at 80 K and at room temperature (insets labeled RT). The relative area of respective spectral components is shown. Fe^{2+}(Si) stands for divalent iron atoms in silicates.

3.3.3 Hydrochemical modeling using PHREEQC

To determine the saturation state of the solutions with respect to minerals detected in the samples as well as those which were previously evidenced to control the chemical composition of pore waters in the Baltic (e.g. Kulik et al., 2000), geochemical modeling was carried out using the PHREEQC software. These involve carbonates (calcite, dolomite, and rhodochrosite), sulfides (pyrite, mackinawite, and greigite), and iron (oxyhydr)oxides (amorphous $Fe(OH)_3$ and goethite). Analytical data were used as the input. Modeling was run for seawater (SW) sampled a few cm above the sediment and for pore waters (PW) occurring within 11–15 cm in the upper part of the sediments (Figure 9). The overlying seawater was in equilibrium with dolomite both at the MET1-REF and MET1-SAL. In contrast, during freshwater seepage, the seawater was supersaturated with respect to dolomite, and its precipitation was thermodynamically allowed. Pore waters showed supersaturation with respect to dolomite for all the samples regardless of whether freshwater seepage was observed or not. Similar were indicated for calcite but the solutions appeared to be less supersaturated (Figure 9). On the con-

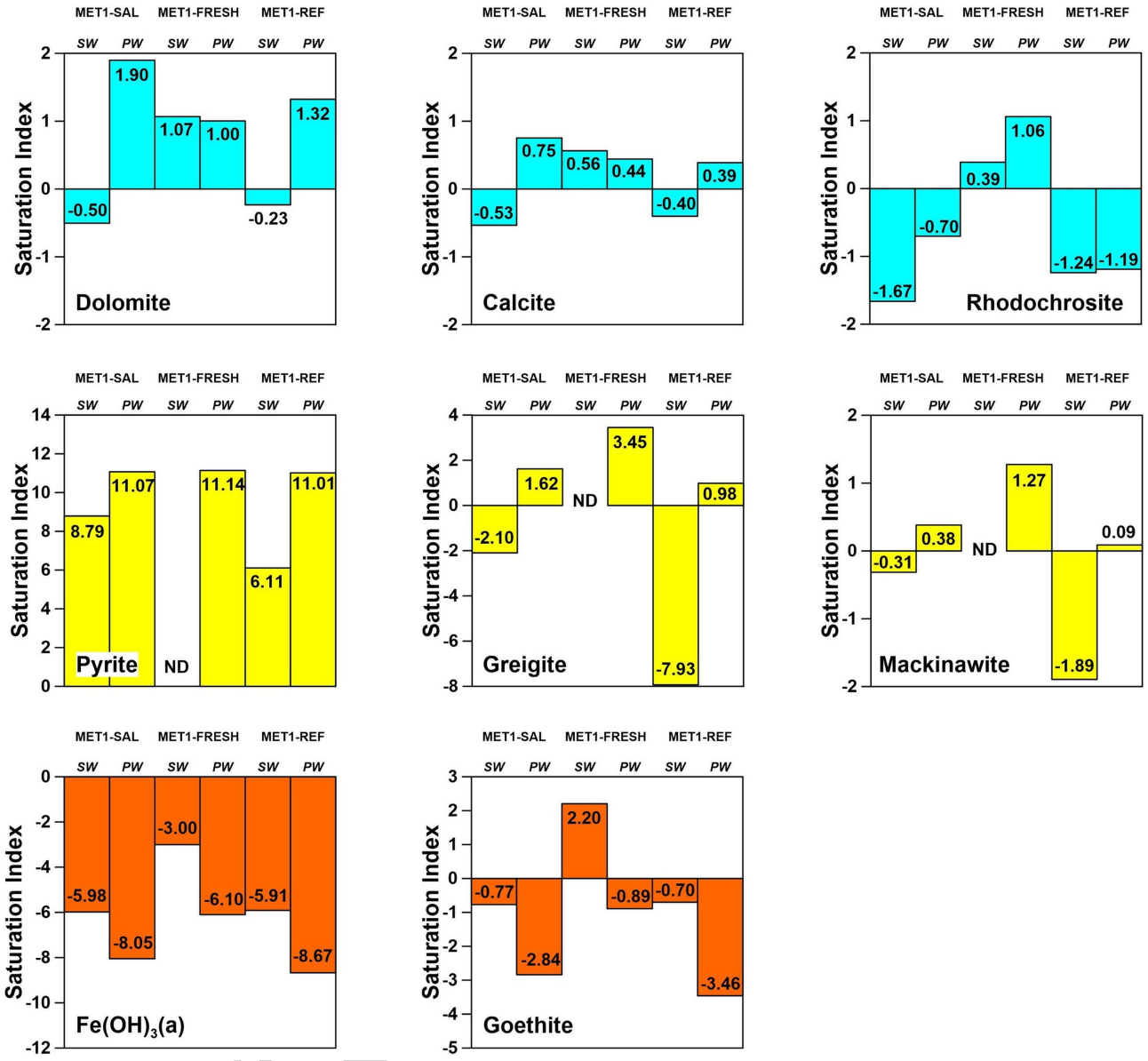

Figure 9. Saturation indices calculated by hydrochemical modeling using PHREEQC. SW and PW denote overlying seawater and pore water, respectively.

trary, rhodochrosite supersaturation was achieved only in MET1-FRESH. For all pore waters and overlying waters analyzed, the modeling indicated high supersaturation with respect to pyrite. On the other hand, supersaturation with respect to metastable sulfides was only reached in pore waters with the highest values in MET1-FRESH. Amorphous ferric hydroxide was undersaturated in all the waters. Goethite was also undersaturated except for overlying water in the pockmark during freshwater seepage.

4. Discussion

The impact of periodic freshwater outflows on mineral-water interactions in the pockmark was studied by comparing the samples taken during freshwater discharge, between the episodes, and samples from the reference site. In the pore waters affected by freshwater, we observed a clear fluoride anomaly (Figure 3e) resulting from the leaching of fluoride minerals found within the limestone-marble and sandy Cretaceous facies underlying the seafloor (Kozerski et al., 1987). This phenomenon has been previously reported and indirectly indicates that the freshwater that feeds the pockmarks is derived from these groundwaters (Idczak et al., 2020; Kurowski et al., 2024).

Freshwater discharge primarily causes the dilution of pore water and seawater near the bottom, as evidenced by the reduction in chloride concentrations (Figure 2a).

Changes in the chemical conditions of the environment affect in turn the taxonomic composition (Figure 4a) and functional profiles (Figure 4b) of microbial communities. Depending on the chemical conditions, the activity of individual groups of microorganisms can shape the course of biogeochemical processes and authigenesis in the sediment. Bacterial metabolic products released into the pore water cause the pore water to become supersaturated with respect to certain mineral phases. These are manifested by the increased presence of authigenic carbonates and the reduced presence of authigenic Fe sulfides.

4.1 Microbiology

Typically, pockmarks appear to have a different microbial composition than their surroundings. This is true for both active pockmarks, where hydrocarbon seeps may be present (Idczak et al., 2020; Whiticar, 2002), and inactive pockmarks (Haverkamp et al., 2014). The freshwater outflow episode could certainly modify the microbial composition, especially of those microorganisms whose metabolism strongly depends on the presence of seawater components. One could expect changes primarily in the Archaea group and sulfate-reducing bacteria. However, Desulfobacteria may have a greater share in the composition of microbial communities in the surface layers of MET1-REF than in the case of MET1-SAL, even though MET1-SAL concerns the episode of saltwater intrusion rich in sulfate. Idczak et al. (2020) showed the results of microbiological studies of the MET1-BH during the freshwater outflow episode in March 2019 (and therefore corresponding exactly to MET1-FRESH). The relative ratios of individual groups of microorganisms are similar (despite the differences resulting from bioinformatic methods and databases). In both MET1-SAL and MET1-BH (the latter from Idczak et al., 2020), the relative contents of Gammaproteobacteria and the ratios are similar. In turn, Alphaproteobacteria are a minority among Proteobacteria, although the differences are slightly more pronounced here. The differences may relate to the increased abundance of microorganisms in the case of a freshwater outflow episode. For example, Methanomicrobia very strongly dominated the archaeal microbial community, which cannot be said about MET1-SAL. On the other hand, the entire profile in MET1-SAL was dominated by Nanoarchaeia. Therefore, the outflow of freshwater in the pockmark certainly affects microbial communities, although it does not cause a 'reshuffling' but can enhance the presence of certain groups of microorganisms. From a microbiological point of view, it seems that the pockmark is a site that differs from the surroundings in both the saltwater intrusion and the freshwater outflow episode. Freshwater discharge can affect the composition of the microbial community by flushing and transporting microorganisms within sediments. Dispersal by advection can cause random variation in community structure, but ultimately the distribution and dynamics of a population depend on selective environmental pressures and interactions between organisms (Justice et al., 2017; Zhai et al., 2022). It seems that changes in porewater salinity modify the activities of the microorganisms present there. Therefore, depending on the conditions at a given time, certain microorganisms that prefer these conditions become dominant in the microbial community.

The influx of water usually significantly modifies the chemical composition of the water and affects microbial composition (Pizzetti et al., 2016; Neubauer et al., 2019). In the case of freshwater intrusion into submarine sediments, depletion of available sulfate is usually observed (Whiticar, 2002). Sulfate in sediments is reduced by sulfate-reducing bacteria (SRB) and archaea (Jørgensen et al., 2001; Rozan et al., 2002). Depletion in sulfate results in an increase in methanogenesis. Indeed, a microbial community with high methanogenic potential was recorded throughout the sediment column at the pockmark. Such potential was lower in the reference profile, which can be explained by differences in sulfate availability and freshwater input. Similarly, differences can be observed in the transformation of sulfur compounds resulting from differences in the composition of microorganisms. However, it is not always possible to distinguish the sulfate reduction zone from the effect of freshwater intrusion (Breuker et al., 2013).

4.2 Geochemistry and mineralogy

Reduction–oxidation reactions mediated by microorganisms have significant impact on the ambient sediment geochemistry (e.g. Morse et al., 1992; Morse and Berner, 1995; Jørgensen et al., 2019; Wang et al., 2020). This is directly reflected in the mineral speciation of Fe and S in the sediment, since these elements (and co-occurring Mn) are strongly redox-sensitive. Reduced sulfate availability due to the infiltration of fresh groundwater meant that biologically induced sulfate reduction, and consequently hydrogen sulfide production, was less intense (Figure 2c), limiting reductive Fe and Mn dissolution. However, Fe and Mn (oxyhydr)oxides could still serve as oxidants in AOM as well as organoclastic reduction (Froelich et al., 1979; Jørgensen, 1982; Sundby et al., 1986; Rozan et al., 2002; Jørgensen and Parkes, 2010; Raiswell and Canfield, 2012) as evidenced by the porewater profiles of Fe^{2+} and Mn^{2+} (Figure 2g.h). The concentrations of Fe^{2+} and Mn^{2+} in the pockmark were higher than at the reference station, where they did not exceed 1.1 µmol/dm^3 for Fe^{2+} and 0.6 µmol/dm^3 for Mn^{2+}. Even without freshwater seepage, Fe^{2+} and Mn^{2+} concentrations in pore water at the pockmark were higher (maximum concentrations were 48 µmol/dm^3 and 23 µmol/dm^3, respectively). Due to the limited availability of sulfate during freshwater outflow, the use of Fe^{3+} and Mn^{4+} as oxidants increased even further. As a result, the concentrations of soluble Fe^{2+} and Mn^{2+}

went up and reached 68 µmol/dm^3 and 133 µmol/dm^3, respectively, during freshwater influx (Figure 2g,h).

As a consequence of freshwater intrusion and pore water dilution in pockmarks, the AOM coupled to sulfate reduction (SO_4^{2-}-AOM) may be constrained by low sulfate concentration, which was previously observed by Brodecka-Goluch et al. (2022) for the nearby pockmark MET1-MP. In active pockmarks, a high demand for electron acceptors causes oxidants other than sulfate to participate in AOM (Thang et al., 2013; Egger et al., 2015). In the marine environments with depleted sulfate and where iron (oxyhydr)oxides are common in surface sediments (e.g. in most regions of the Gulf of Gdańsk) they may become additional significant oxidants for the AOM (Sivan et al., 2011; Riedinger et al., 2014; Kurowski et al., 2024). Their involvement in this process may generate substantial changes to the iron cycle in marine sediments (Beal et al., 2009; Yang et al., 2021) and subsequently produce different minerals in sediments (Teichert et al., 2005; Akam et al., 2020).

The response of the sediment to freshwater outflows is much more difficult to observe because, unlike the concentrations of pore water constituents, the content of mineral phases cannot be quantified with comparable precision. In addition, differences between freshwater-impacted sediments and the reference station in the amount and formation of authigenic rather than detrital minerals, which are less common, should be sought. Indeed, the type and content of detrital (alumino)silicates were similar in sediments from all stations. On the other hand, differences in the amount of authigenic carbonates and sulfides became apparent. These differences were consistent with the differences in the chemical composition of sediments and pore waters described above. However, when analyzing the results of thermodynamic modeling, it should be kept in mind that the value of the obtained saturation indices for a given mineral phase could have been affected by the method of pore water extraction. Extraction of pore water by vacuum filtration may lead to degassing of CO_2 from the fluids. This, in turn, may cause a shift in pH, and consequently affect ionic equilibrium in the solution and ion speciation (Schrum et al., 2012). To consider the effect of CO_2 degassing on pH and ion speciation, additional PHREEQC simulations of the SI response to pH variation were carried out to evaluate the effect of pH change resulting from partial or complete degassing of CO_2 (Supplementary Material, Figure S2). The results demonstrate that the observed relationships between the samples and the SI sign remain unchanged.

In the case of detrital (alumino)silicates, the only manifestation of the sedimentary response to disequilibrium is the increase in dSi in pore solutions observed during freshwater discharge (Figure 3h). Mineralization of the large amount of organic matter deposited in the pockmark leads to an increase in CO_2 concentration. This can intensify the weathering of some detrital aluminosilicates, including feldspars (Mackenzie and Lerman, 2006). Thus, aluminosilicate weathering may be another factor, in addition to biogenic silica degradation, causing an increase in dSi concentrations in pore waters. Consequently, the concentration of dSi in the pockmark was higher than at the reference station (Figure 3h) both during freshwater outflow and later when the pockmark depression was refilled with salt water. A noticeably higher dSi concentration was recorded during freshwater outflow (Figure 3h). This may be related to a shift in the CH_4 production pathway as a result of freshwater conditions. Under such conditions, acetate fermentation dominates (Whiticar et al., 1986), producing CO_2 in addition to CH_4, which in turn can cause weathering of aluminosilicates and promote high dSi concentration.

Mössbauer spectroscopy indicates that almost all the iron present in the sediments is in the reduced form of Fe^{2+}, mainly in pyrite. Pyrite formation is confirmed by the presence of strongly reducing conditions in this environment. The presence of pyrite framboids is often explained by formation with microbial involvement (Maclean et al., 2008; Wacey et al., 2015, Picard et al., 2016). There are also more recent works indicating that framboids can be formed by inorganic processes (Wilkin and Barnes, 1997; Frankel and Bazylinski, 2003; Runge et al., 2024), especially via metastable amorphous FeS, greigite, and mackinawite intermediates (Wang and Morse, 1996). In the pockmark, pyrite is less abundant and more often forms dispersed grains rather than framboids, despite virtually the same pyrite saturation indices as at the reference station and distinctly higher supersaturation with respect to metastable sulfides (greigite and mackinawite) than at the reference station (Figure 9). This is the result of reduced availability of H_2S due to less intense sulfate reduction resulting from freshwater intrusions. On the other hand, lower saturation with respect to precursor metastable sulfides with simultaneous supersaturation with respect to pyrite (observed at MET1-SAL and MET1-REF) might suggest hindering of direct nucleation from porewater. Pyrite formation was affected by microorganisms as demonstrated by Thiel et al. (2019) who showed that microbially catalyzed redox processes where hydrogen sulfide reacts with FeS lead to formation of pyrite and hydrogen. On the one hand this process is driven by sulfate-reducers producing H_2S, on the other hand, the process is controlled by hydrogenotrophic methanogens which can utilize H_2. Both sulfate reduction and hydrogenotrophic methanogenesis are typical for marine and brackish environments. Therefore, coupling these two microbial factors controlling the pyrite formation process may be particularly effective when freshwater seepages do not occur. As a result, more framboids that may indicate microbial mediation should be expected in MET1-REF than in MET1-FRESH.

Variations in carbonate concentrations are inversely correlated with changes in sulfate concentrations in pore

waters. Increased precipitation of calcium and magnesium carbonates is observed in the sediment affected by freshwater input. Hydrochemical modeling (Figure 9) indicates that pore waters are slightly supersaturated relative to calcite and dolomite and seawater becomes supersaturated during freshwater outflow. Supersaturation with respect to rhodochrosite is also achieved only at MET1-FRESH. This may be related to an increase in the concentration of DIC in the upper part of the profile (Figure 2e), which is probably associated with intensive organic matter degradation processes and increased CO_2 production resulting from microbially induced AOM, pronounced during freshwater seepage (Figure 2d). These processes may cause supersaturation of pore waters with carbonate phases and increase the content of particulate inorganic carbon in CH_4-bearing sediments compared to CH_4-free sediments, which has been previously noted in the Gdańsk Basin (Brodecka-Goluch and Łukawska-Matuszewska, 2018). These observations are consistent with the mineral composition of the sediments: the presence of authigenic carbonates was higher at MET1-FRESH than at the reference station.

Significant is not only the increase in the amount of carbonate minerals in the sediments affected by freshwater discharge but also the fact that carbonates precipitate in these sediments in the form of CMC. The authigenic nature is evidenced by SEM observations showing euhedral, automorphic, rather than detrital morphology. Jakobsen and Postma (1989) reported dolomite crystals in the center of rhodochrosite aggregates in the Baltic, suggesting that rhodochrosite had nucleated upon preexisting dolomite, the detrital nature of which was inferred based on its fractured appearance. This is, however, probably not our case since the CMC crystals found in the pockmark were perfectly euhedral and did not reveal any fractures or any transport-related features (Figur 7c,d). If the observed CMC crystals were dolomite, this would have important geochemical implications. Dolomite, although a very common mineral on Earth, is very difficult to research and still holds many secrets. Direct precipitation of dolomite from aqueous solutions is usually limited by kinetic barriers and is not observed even from supersaturated solutions (Land, 1998). The limited ability of dolomite to crystallize under ambient conditions has been the subject of scientific debate for many years (see, for example, McKenzie, 1991; Baldermann et al., 2015; Gregg et al., 2015; García-Ruiz, 2023). So far, experimental attempts to precipitate dolomite crystals from aqueous solutions have been considered unsuccessful, rather forming variations of magnesium calcite (see e.g., Gregg et al., 2015). It seems that dolomite precipitation catalyzed by microbial activity is possible (Vasconcelos et al., 2005). There is also evidence that microbes (e.g., sulfate-reducing bacteria and methanogens) can promote the precipitation of primary dolomite under seafloor conditions (Xu et al., 2019). Furthermore, it is observed that such primary dolomite produced by microorganisms is often enriched in Fe^{2+}. These findings match our observations. Baker and Kastner (1981) also concluded that the decrease of dissolved SO_4^{2-} (by calcium sulfate precipitation and bacterial SO_4^{2-} reduction or through mixing of seawater with freshwater) stimulates dolomite formation, even though their conclusions were based on experiments at 200°C. Dissolved sulfate is an efficient inhibitor of dolomite precipitation because it forms a $MgSO_4^0$ complex even at low SO_4^{2-} levels (Baker and Kastner, 1981; Kastner, 1984, Magalhães et al., 2012). There are also reports that sulfate is not an effective inhibitor, at least during bacterial-mediated precipitation (Sánchez-Román et al., 2009). In sediments rich in organic matter, the demand for O_2 for OM decomposition exceeds its availability. Consequently, other electron acceptors, including sulfate, are involved in the process, further lowering sulfate concentration already reduced due to freshwater seepage (Figure 2b). Sulfate is also consumed during AOM. Both processes, dissimilatory sulfate reduction and AOM with sulfate, cause a strong increase in the concentration of DIC in pore waters (Figure 2e). In turn, higher bicarbonate supersaturation and lower sulfate concentrations observed within the pockmark have an impact on Mg ionic speciation and might increase the available magnesium for dolomite precipitation. Our geochemical modeling revealed a reduction in the share of $MgSO_4^0$ speciation among all magnesium forms during freshwater outflows (data not presented). It seems that other specific physicochemical and sedimentological features of the pockmark environment also favor the possibility of dolomite formation. These include: (i) sediments rich in OM, (ii) methanogenesis and subsequent AOM with iron and sulfate as important DIC sources, (iii) higher Ca^{2+} concentrations (Figure 3c), and (iv) the exchange of NH_4^+ (produced during anaerobic OM oxidation) for Mg^{2+} from clay minerals (Baker and Kastner, 1981). Kelts and McKenzie (1982) reported dolomite formation in deep-sea sediments with similar features, i.e. low sulfate concentration, rich in DIC and NH_4^+, commonly in conjunction with zones of methanogenesis. They concluded that Ca^{2+} and Mg^{2+} are derived from interstitial waters, and a rise in NH_4^+ adds magnesium to pore water by exchange with smectite mixed-layer clay. Moreover, the recent work of Kim et al. (2023) demonstrates that cycling between undersaturation and supersaturation (which in our case is induced by fluctuating freshwater seepage) favors dolomite growth, accelerating it by a few orders of magnitude. Therefore, many features of the pockmark environment appear to favor dolomite precipitation.

5. Conclusions

The differences between pockmark depressions and their surroundings arise mostly from gas and freshwater outflows. Freshwater modifies chemical composition of pore water in the sediment and affects both the degree of supersaturation of solutions relative to sediment minerals and

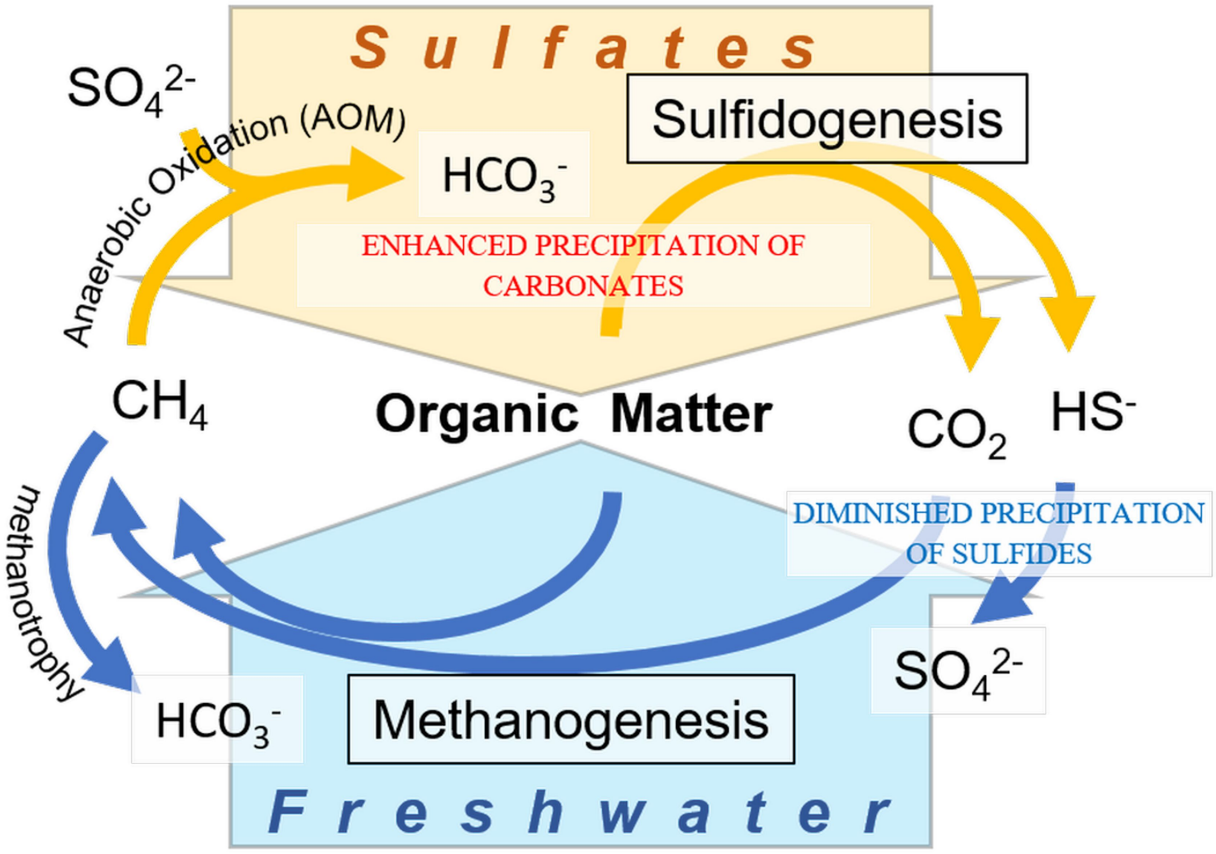

Figure 10. Possible microbial processes controlled by two main factors in the system studied. Usually, sulfidogenesis predominates in the shallow sea sediment. Methanogenesis may occur in deeper sediments and the generated methane may undergo AOM closer to the surface. Freshwater intrusion strongly disturbs this process, enabling methanogenesis even within the entire sediment column. Then, methanotrophic processes may also be intensified.

the composition and functioning of the microbial system. In such cases, both microbial processes and the associated formation of mineral phases in the sediment can be controlled by two main factors: (1) downward sulfate influx from seawater overlying the sediment and (2) upward freshwater intrusion. With the other parameters held constant, these two factors play a key role in the system.

A conceptual model of the processes is proposed in Figure 10. In pockmark sediments undisturbed by freshwater, the co-occurrence of sulfate reduction and anaerobic oxidation of methane (AOM) generates carbonate and sulfide ions, causing the precipitation of sulfide and carbonate minerals. Freshwater seepages can cause sulfate depletion of pore waters, affecting both sulfate reduction (by lowering the concentrations of available sulfate) and methanogenesis (because the activity of sulfate-reducing bacteria has an inhibitory effect on methanogenic activity). Therefore, an increased methanogenesis can occur in sediments disturbed by freshwater intrusions. This is followed by AOM which increases the supply of carbonate contributing to the crystallization of carbonate minerals. As intrusion of freshwater reduces the availability of sulfate, which is usually the most important oxidant used by methane-oxidizing microorganisms, the importance of Fe (oxyhydr)oxides as an alternative oxidant in AOM increases. Excess of Fe^{2+} in pore waters can precipitate in the form of authigenic carbonates, facilitated by low concentrations of hydrogen sulfide, the production of which is limited under a low supply of sulfate. In addition, insufficient availability of hydrogen sulfide inhibits the formation of authigenic sulfides. Therefore, the mineral composition of sediments in pockmarks with freshwater intrusion may differ from sediments with no freshwater intrusion in terms of increased carbonate and decreased sulfide minerals presence. This model has been derived based on the analysis of a single layer of the sediment. The model will be further verified through comprehensive studies in the entire sediment profile of the pockmarks.

An unusual peculiarity of the studied environment is the possibility of precipitation of carbonate minerals in the form of euhedral crystals of authigenic dolomite. This is a rare phenomenon so further studies are needed for unambiguous identification of these Ca-Mg carbonates. A comparison of SEM images with literature data shows that such well-developed, relatively large microcrystals of dolomite as those found in the sediments of the studied pockmarks are exceptional. They may be comparable to dolomites found in cores from the Deep-Sea Drilling Project. Although that study showed that euhedral dolomite is quite common in deep-sea sediments (up to 1%), it was thought to be a product of chemical precipitation during early sediment diagenesis rather than primary formation during sediment deposition on the sea floor (Lumsden, 1988). Therefore, the authigenic CMC found in pockmarks should be considered unique and will be the subject of further studies using micro-Raman spectroscopy and electron diffraction by transmission electron microscopy.

Acknowledgements

The mineralogical and microbiological parts of the study as well as hydrogeochemical modeling were funded by the National Science Centre, Poland (Project No. UMO-2022/45/B/ST10/00395). The authors thank the crew of the r/v *Oceanograf*. We also thank two anonymous reviewers whose constructive and valuable comments allowed improving the quality and clarity of the manuscript.

Supplementary material

Supplementary material associated with this article can be found here.

Conflict of interest

None declared.

References

Aitchison, J., 1982. *The Statistical Analysis of Compositional Data*. J. R. Stat. Soc. Ser. B Method. 44, 139–177. https://www.jstor.org/stable/2345821

Akam, S.A., Coffin, R.B., Abdulla, H.A.N., Lyons, T.W., 2020. *Dissolved organic carbon pump in methane-charged shallow marine sediments: state of the art and new model perspectives*. Front. Mar. Sci. 7, 206. https://doi.org/10.3389/fmars.2020.00206

Babicki, S., Arndt, D., Marcu, A., Liang, Y., Grant, J.R., Maciejewski, A., Wishart, D.S., 2016. *Heatmapper: web-enabled heat mapping for all*. Nucleic Acids Res. 44, W147–W153. https://doi.org/10.1093/nar/gkw419

Baker, P.A., Kastner, M., 1981. *Constraints on the formation of sedimentary dolomite*. Science 213, 214–216. https://doi.org/10.1126/science.213.4504.21

Baldermann, A., Deditius, A.P., Dietzel, M., Fichtner, V., Fischer, C., Hippler, D., Leis, A., Baldermann, C., Mavromatis, V., Stickler, C.P., Strauss, H., 2015. *The role of bacterial sulfate reduction during dolomite precipitation: Implications from Upper Jurassic platform carbonates*. Chem. Geol. 412, 1–14. https://doi.org/10.1016/j.chemgeo.2015.07.020

Beal, E.J., House, C.H., Orphan, V.J., 2009. *Manganese- and iron-dependent marine methane oxidation*. Science 325, 184–187. https://doi.org/10.1126/science.11699

Błachowski, A., Ruebenbauer, K., Żukrowski, J., Górnicki, R., 2008. *Early design stage of the MsAa-4 Mössbauer spectrometer*. Acta Phys. Pol. A 114, 1707–1713. https://doi.org/10.12693/APhysPolA.114.1707

Boogaart, K.G. van den, Tolosana-Delgado, R., Bren, M., 2023. Compositions: Compositional Data Analysis.

Breuker, A., Stadler, S., Schippers, A., 2013. *Microbial community analysis of deeply buried marine sediments of the New Jersey shallow shelf (IODP Expedition 313)*. FEMS Microbiol. Ecol. 85, 578–592. https://doi.org/10.1111/1574-6941.12146

Brodecka-Goluch, A., Idczak, J., Gorska, N., Bolałek, J., 2020. *Geophysical and geochemical characteristics of four different pockmark sites located in the Gdańsk Basin*. 3rd Baltic Earth Conference Earth System Changes and Baltic Sea Coasts, 89–90.

Brodecka-Goluch, A., Łukawska-Matuszewska, K., 2018. *Porewater dissolved organic and inorganic carbon in relation to methane occurrence in sediments of the Gdańsk Basin (southern Baltic Sea)*. Cont. Shelf Res. 168, 11–20. https://doi.org/10.1016/j.csr.2018.08.008

Brodecka-Goluch, A., Łukawska-Matuszewska, K., Kotarba, M.J., Borkowski, A., Idczak, J., Bolałek, J., 2022. *Biogeochemistry of three different shallow gas systems in continental shelf sediments of the South-Eastern Baltic Sea (Gulf of Gdańsk): carbon cycling, origin of methane and microbial community composition*. Chem. Geol. 597, 120799. https://doi.org/10.1016/j.chemgeo.2022.120799

Burton, E.A., 1993. *Controls on marine carbonate cement mineralogy: Review and reassessment*. Chem. Geol. 105, 163–179. https://doi.org/10.1016/0009-2541(93)90124-2

Byrne, J.M., Kappler, A., 2019. *Mössbauer spectroscopy*. [In:] Kenney, J.P.L., Veeraramani, H., Alessi, D.S., (Eds.), *Analytical Geomicrobiology. A Handbook of Instrumental Techniques*, Cambridge Univ. Press, 314–337.

Chen, S., Zhou, Y., Chen, Y., Gu, J., 2018. *fastp: an ultra-fast all-in-one FASTQ preprocessor*. Bioinformatics 34, i884–i890. https://doi.org/10.1093/bioinformatics/bty560

Cole, D., Stewart, S.A., Cartwright, J.A., 2000. *Giant irregular pockmark craters in the Palaeogene of the outer Moray*

Firth basin, UK North Sea. Mar. Pet. Geol. 17, 563–577. https://doi.org/10.1016/S0264-8172(00)00013-1

Dowgiałło, J., Kozerski, B., 1975. *Wody wgłębne podłoża Bałtyku*. Stud. Mat. Oceanol. 11, 55–66 (in Polish).

Dyar, M.D., Agresti, D.G., Schaefer, M.W., Grant, C.A., Sklute, E.C., 2006. *Mössbauer spectroscopy of Earth and planetary materials*. Ann. Rev. Earth Planet. Sci. 34, 83–125. https://doi.org/10.1146/annurev.earth.34.031405.125049

Egger, M., Rasigraf, O., Sapart, C.J., Jilbert, T., Jetten, M.S.M., Röckmann, T., van der Veen, C., Bândă, N., Kartal, B., Ettwig, K.F., Slomp, C.P., 2015. *Iron-mediated anaerobic oxidation of methane in brackish coastal sediments*. Environ. Sci. Technol. 49, 277–283. https://doi.org/10.1021/es503663z

Ehlert von Ahn, C.M., Dellwig, O., Szymczycha, B., Kotwicki, L., Rooze, J., Endler, R., Escher, P., Schmiedinger, I., Sültenfuß, J., Diak, M., Gehre, M., Struck, U., Vogler, S., Böttcher, M.E., 2024. *Submarine groundwater discharge into a semi-enclosed coastal bay of the southern Baltic Sea: A multi-method approach*. Oceanologia 66 (1), 111–138. https://doi.org/10.1016/j.oceano.2024.01.001

Falkowska, L., Piekarek-Jankowska, H., 1999. *Submarine seepage of fresh groundwater: disturbance in hydrological and chemical structure of the water column in the Gdańsk Basin*. J. Mar. Sci. 56, 153–160.

Frankel, R.B., Bazylinski, D., 2003. *Biologically Induced Mineralization by Bacteria*. Rev. Mineral. Geochemi. 54, 95–114.

Froelich, P.N., Klinkhammer, G.P., Bender, M.L., Luedtke, N.A., Heath, G.R., Cullen, D., Dauphin, P., Hammond, D., Hartman, B., Maynard, V., 1979. *Early oxidation of organic matter in pelagic sediments of the eastern equatorial Atlantic: suboxic diagenesis*. Geochim. Cosmochim. Acta 43, 1075–1090. https://doi.org/10.1016/0016-7037(79)90095-4

García-Ruiz, J.M., 2023. *A fluctuating solution to the dolomite problem*. Science 382, 883–884. https://doi.org/10.1126/science.adl1734

Giovanelli, D., D'Errico, G., Fiorentino, F., Fattorini, D., Regoli, F., Angeletti, L., Bakran-Petricioli, T., Vetriani, C., Yücel, M., Taviani, M., Manini, E., 2016. *Diversity and distribution of procaryotes within a shallow-water pockmark field*. Front. Microbiol. 7, 941. https://doi.org/10.3389/fmicb.2016.00941

Greinert, J., Bohrmann, G., Suess, E., 2001. *Gas hydrate-associated carbonates and methane venting at Hydrate Ridge: Classification, distribution and origin of authigenic lithologies*. [In:] Paull, C., Dillon, W. (Eds.), *Natural Gas Hydrates: Occurrence, Distribution, and Detection*, Am. Geophys. Union. Wash. Monogr. 124, 99–113.

Grasshoff, K., Kremling, K., Ehrhardt, M., 1999. *Methods of Seawater Analysis*, 3rd edn., Wiley-VCH, Weinheim, 600 pp.

Gregg, J.M., Bish, D.L., Kaczmarek, S.E., Machel, H.G., 2015. *Mineralogy, nucleation and growth of dolomite in the laboratory and sedimentary environment: A review*. Sedimentology 62, 1749–1769. https://doi.org/10.1111/sed.12202

Haverkamp, T.H.A., Hammer, Ø., Jakobsen, K.S., 2014. *Linking geology and microbiology: Inactive pockmarks affect sediment microbial community structure*. PLOS One 9 (1), e85990. https://doi.org/10.1371/journal.pone.0085990

Hoffmann, J., Schneider von Deimling, J., Schröder, J., Schmidt, M., Held, P., Crutchley, G., Scholten, J., Gorman, A., 2020. *Complex Eyed Pockmarks and Submarine Groundwater Discharge Revealed by Acoustic Data and Sediment Cores in Eckernförde Bay, SW Baltic Sea*. Geochem. Geophy. Geosy. 21, e2019GC008825. https://doi.org/10.1029/2019GC008825

Hovland, M., Judd, A.G., 1988. *Seabed Pockmarks and Seepages*. Graham and Trotman Inc. Sterling House, London, 293 pp.

Hung, C-W., Huang, K-H., Shih, Y-Y., Lin, Y-S., Chen, H-H., Wang, C-C., Ho, C-Y., Hung, C-C., Burdige, D.J., 2016. *Benthic fluxes of dissolved organic carbon from gas hydrate sediments in the northern South China Sea*. Sci. Rep. 6, 29597. https://doi.org/10.1038/srep29597

Idczak, J., Brodecka-Goluch, A., Łukawska-Matuszewska, K., Graca, B., Gorska, N., Klusek, Z., Pezacki, P., Bolałek, J., 2020. *A geophysical, geochemical and microbiological study of a newly discovered pockmark with active gas seepage and submarine groundwater discharge (MET1-BH, central Gulf of Gdańsk, southern Baltic Sea)*. Sci. Tot. Environ. 742, 140306. https://doi.org/10.1016/j.scitotenv.2020.140306

Iasakov, T.R., Kanapatskiy, T.A., Toshchakov, S.V., Korzhenkov, A.A., Ulyanova, M.O., Pimenov, N.V., 2021. *The Baltic Sea methane pockmark microbiome: The new insights into the patterns of relative abundance and ANME niche separation*. Mar. Environ. Res. 173, 105533. https://doi.org/10.1016/j.marenvres.2021.105533

IHO S-44, 2020. *International Hydrographic Organization Standards for Hydrographic Surveys S-44*, Edition 6.1.0, available online. https://iho.int/uploads/user/pubs/standards/s-44/S-44_Edition_6.1.0.pdf;access17/11/2025

Jakobsen, R., Postma, D., 1989. *Formation and solid solution behavior of Ca-rhodochrosites in marine muds of the Baltic deeps*. Geochim. Cosmochim. Acta 53, 2639–2648. https://doi.org/10.1016/0016-7037(89)90135-X

Jakobsson, M., O'Regan, M., Gyllencreutz, R., Flodén, T., 2016. *Seafloor terraces and semi-circular depressions related to fluid discharge in Stockholm Archipelago, Baltic Sea*. [In:] Dowdeswell, J.A., Canals, M., Jakobsson, M., Todd, B.J., Dowdeswell, E.K., Hogan, K.A. (Eds.), *Atlas of Submarine Glacial Landforms: Modern, Quaternary and Ancient*. Geological Society, London, Memoirs Vol. 46, 305–306.

Jaśniewicz, D., Klusek, Z., Brodecka-Goluch, A., Bolałek, J., 2019. *Acoustic investigations of shallow gas in the southern Baltic Sea (Polish exclusive Economic Zone): A review*. Geo-Mar. Lett. 39, 1–17. https://doi.org/10.1007/s00367-018-0555-5

Jørgensen, B.B., 1982. *Mineralization of organic matter in the sea bed – the role of sulphate reduction*. Nature 296, 643–645. https://doi.org/10.1038/296643a0

Jørgensen, B.B., Findlay, A.J., Pellerin, A., 2019. *The biogeochemical sulfur cycle of marine sediments*. Front. Microbiol. 10, 849. https://doi.org/3389/fmicb.2019.00849

Jørgensen, B.B., Parkes, R.J., 2010. *Role of sulfate reduction and methane production by organic carbon degradation in eutrophic fjord sediments (Limfjorden, Denmark)*. Limnol. Oceanogr. 55, 1338–1352. https://doi.org/10.4319/lo.2010.55.3.1338

Jørgensen, B.B., Weber, A., Zopfi, J., 2001. *Sulfate reduction and anaerobic oxidation in Black Sea sediments*. Deep-Sea Res. Pt. I 48, 2097–2120. https://doi.org/10.1016/S0967-0637(01)00007-3

Judd, A., Hovland, M., 2007. *Seabed Fluid Flow: The Impact on Geology, Biology, and the Marine Environment*. Cambridge University Press, 492 pp.

Justice, N.B., Sczesnak, A., Hazen, T.C., Arkin, A.P., 2017. *Environmental selection, dispersal, and organism interactions shape community assembly in high-throughput enrichment culturing*. Appl. Environ. Microbiol. 83, e01253-17. https://doi.org/10.1128/AEM.01253-17

Kastner, M., 1984. *Control of dolomite formation*. Nature 311, 410–411. https://doi.org/10.1038/311410b0

Kelts, K., McKenzie, J.A., 1982. *Diagenetic dolomite formation in Quaternary anoxic diatomaceous muds of deep sea drilling project Leg 64, Gulf of California*. [In:] Curray, J.R., Moore, D.G., et al. (Eds.), *Initial Reports of the Deep Sea Drilling Project*, U.S. Govt. Printing Office, 64, 553–569. https://doi.org/10.2973/dsdp.proc.64.110.1982

Kim, J., Kimura, Y., Puchala, B., Yamazaki, T., Becker, U., Sun, W., 2023. *Dissolution enables dolomite crystal growth near ambient conditions*. Science 382, 915–920. https://doi.org/10.1126/science.adi3690

King, L.H., MacLean, B., 1970. *Pockmarks on the Scotian Shelf*. GSA Bull. 81, 3141–3148. https://doi.org/10.1130/0016-7606(1970)81[3141:POTSS]2.0.CO;2

Knittel, K., Boetius, A., Lemke, A., Eilers, H., Lochte, K., Pfannkuche, O., Linke, P., Amann, R., 2003. *Activity, distribution, and diversity of sulfate reducers and other bacteria in sediments above gas hydrate (Cascadia Margin, Oregon)*. Geomicrobiol. J. 20, 269–294. https://doi.org/10.1080/01490450303896

Kozerski, B., Macioszczyk, A., Pazdro, Z., Sadurski, A., 1987. *Fluoride in groundwaters of the Gdańsk region*. Ann. Soc. Geol. Pol. 57, 349–374 (in Polish).

Kulik, D.A., Kersten, M., Heiser, U., Neumann, T., 2000. *Application of Gibbs energy minimization to model early-diagenetic solid-solution aqueous-solution equilibria involving authigenic rhodochrosites in anoxic Baltic Sea sediments*. Aq. Geochem. 6, 147–199. https://doi.org/10.1023/A:1009694703207

Kurowski, S., Łukawska-Matuszewska, K., Čović, A., Jozić, D., Brodecka-Gołuch, A., 2024. *Effects of pockmark activity on iron cycling and mineral composition in continental shelf sediments (southern Baltic Sea)*. Biogeochemistry 167, 135–154. https://doi.org/10.1007/s10533-024-01127-1

Land, L.S. 1998. *Failure to precipitate dolomite at 25 °C from dilute solution despite 1000-fold oversaturation after 32 years*. Aquat. Geochem. 4, 361–368. https://doi.org/10.1023/A:1009688315854

Loncke, L., Mascle, J., 2004. *Mud volcanoes, gas chimneys, pockmarks and mounds in the Nile deep-sea fan (eastern Mediterranean): geophysical evidence*. Mar. Pet. Geol. 21, 669–689. https://doi.org/10.1016/j.marpetgeo.2004.02.004

Louca, S., Parfrey, L.W., Doebeli, M., 2016. *Decoupling function and taxonomy in the global ocean microbiome*. Science 353, 1272–1277. https://doi.org/10.1126/science.aaf4507

Lu, J., Breitwieser, F.P., Thielen, P., Salzberg, S.L., 2017. *Bracken: estimating species abundance in metagenomics data*. Peer J. Comput. Sci. 3, e104. https://doi.org/10.7717/peerj-cs.104

Lu, J., Rincon, N., Wood, D.E., Breitwieser, F.P., Pockrandt, C., Langmead, B., Salzberg, S.L., Steinegger, M., 2022. *Metagenome analysis using the Kraken software suite*. Nat. Protoc. 17, 2815–2839. https://doi.org/10.1038/s41596-022-00738-y

Lumsden, D.N., 1988. *Characteristics of deep marine dolomite*. J. Sediment. Petrol. 58, 1023–1031. https://doi.org/10.1306/212F8EEF-2B24-11D7-8648000102C1865D

Łukawska-Matuszewska, K., 2016. *Contribution of non-carbonate inorganic and organic alkalinity to total measured alkalinity in pore waters in marine sediments (Gulf of Gdansk, S-E Baltic Sea)*. Mar. Chem. 186, 211–220. https://doi.org/10.1016/j.marchem.2016.10.002

Łukawska-Matuszewska, K., Brocławik, O., Brodecka-Goluch, A., Rzepa, G., Manecki, M., Bolałek, J., 2022. *Biogeochemical and mineralogical effects of Fe-P-S dynamics in sediments of continental shelf sea: Impact of salinity, oxygen conditions, and catchment area characteristics*. Sci. Total Environ. 807, 151035. https://doi.org/10.1016/j.scitotenv.2021.151035

Magalhães, V.H., Pinheiro, L.M., Ivanov, M.K., Kozlova, E., Blinova, V., Kolganova, J., Vasconcelos, C., McKenzie, J.A., Bernasconi, S.M., Kopf, A.J., Díaz-del-Río, V., González, F.J., Somoza, L., 2012. *Formation processes of methane-derived authigenic carbonates from the Gulf of Cadiz*. Sediment. Geol. 243–244, 155–168. https://doi.org/10.1016/j.sedgeo.2011.10.013

McKenzie, J.A., 1991. *The dolomite problem: an outstanding controversy*. [In:] Muller, D.W., Weisser, H., McKenzie, J.A. (Eds.). *Controversies in Modern Geology*. Academic Press, New York, 490 pp.

Mackenzie, F.T., Lerman, A., 2006. *Weathering and Consumption of CO2*. [In:] *Carbon in the Geobiosphere – Earth's Outer Shell*. Topics in Geobiology Vol. 25, Springer, Dordrecht, 225–254.

Maclean, L.C.W., Tyliszczak, T., Gilbert, P.U.P.A., Zhou, D., Pray, T.J., Ostott, T.C., Southam, G., 2008. *A high-resolution chemical and structural study of framboidal pyrite formed within a low-temperature bacterial biofilm*. Geobiology 6, 471–480. https://doi.org/10.1111/j.1472-4669.2008.00174.x

Majewski, A., 1990. *Morphometry and hydrography of the catchment area*. [In:] Majewski, A. (Ed.), *The Gulf of Gdańsk*. Geol. Publ., Warsaw, 7–19 (in Polish).

Majewski, P., Klusek, Z., 2014. *Parameters of echo signals originated from a gas seepage site in the southern Baltic Sea*. Hydroacoustics 17, 143–150.

Matciak, M., Misiewicz, M.M., Szymczycha, B., Idczak, J., Tęgowski, J., Diak, M., 2024. *Pockmarks and associated fresh submarine groundwater discharge in the seafloor of Puck Bay, southern Baltic Sea*. Sci. Total Environ. 942, 173617. https://doi.org/10.1016/j.scitotenv.2024.173617

Mavromatis, V., Botz, R., Schmidt, M., Liebetrau, V., Hensen, C., 2012. *Formation of carbonate concretions in surface sediments of two mud mounds offshore Costa Rica: a stable isotope study*. Int. J. Earth Sci. 103, 1831–1844. https://doi.org/10.1007/s00531-012-0843-7

Moore, D.M., Reynolds, Jr. R.C., 1997. *X-ray Diffraction and the Identification and Analysis of Clay Minerals*. 2nd Edn., Oxford Univ. Press, Oxford, 378 pp.

Morse, J.W., Berner, R.A., 1995. *What determines sedimentary C/S ratios?*. Geochim. Cosmochim. Acta 59, 1073–1077. https://doi.org/10.1016/0016-7037(95)00024-T

Morse, J.W., Cornwell, J.C., Arakaki, T., Lin, S., Huerta-Diaz, M.A., 1992. *Iron sulfide and carbonate mineral diagenesis in Baffin Bay*, Texas. J. Sed. Res. 62, 671–680. https://doi.org/10.1306/D4267983-2B26-11D7-8648000102C1865D

Neubauer, S.C., Piehler, M.F., Smyth, A.R., Franklin, R.B., 2019. *Saltwater intrusion modifies microbial community structure and decreases denitrification in tidal freshwater marshes*. Ecosystems 22, 912–928. https://doi.org/10.1007/s10021-018-0312-7

O'Reilly, S.S., Jordan, S.F., Monteys, X., Simpson, A.J., Allen, C.C.R., Szpak, M.T., Murphy, B.T., McCarron, S.G., Soong, R., Wu, B., Jenne, A., Grey, A., Kelleher, B.P., 2021. *Production of methane and gaseous compounds by surface microbial activity in small pockmark field, Dunmanus Bay, Ireland*. Estuar. Coast. Shelf Sci. 255, 107340. https://doi.org/10.1016/j.ecss.2021.107340

Orcutt, B., Boetius, A., Elvert, M., Samarkin, V., Joye, S.B., 2005. *Molecular biogeochemistry of sulfate reduction, methanogenesis and the anaerobic oxidation of methane at Gulf of Mexico cold seeps*. Geochim. Cosmochim. Acta 69, 4267–4281. https://doi.org/10.1016/j.gca.2005.04.012

Palarea-Albaladejo, J., Martín-Fernández, J.A., 2015. *zCompositions – R package for multivariate imputation of left-censored data under a compositional approach*. Chemom. Intell. Lab. Syst. 143, 85–96. https://doi.org/10.1016/j.chemolab.2015.02.019

Parkhust, D.L., Appelo, C.A.J., 2013. *Description of Input and Examples for PHREEQC Version 3 – A Computer Program for Speciation, Batch-Reaction, One-Dimensional Transport, and Inverse Geochemical Calculations*. US Geological Survey Techniques and Methods, Book 6, Chapter A43, 497 pp. http://pubs.usgs.gov/tm/06/a43

Peckmann, J., Reimer, A., Luth, U., Luth, C., Hansen, B.T., Heinicke, C., Hoefs, J., Reitner, J., 2001. *Methane-derived carbonates and authigenic pyrite from the northwestern Black Sea*. Mar. Geol. 177, 129–150. https://doi.org/10.1016/S0025-3227(01)00128-1

Picard, A., Gatman, A., Girguis, P.R., 2016. *What do we really know about the role of microorganisms in iron sulfide mineral formation*. Front. Earth Sci. 4, 68. https://doi.org/10.3389/feart.2016.00068

Piekarek-Jankowska, H., 1994. *Zatoka Pucka jako obszar drenażu wód podziemnych*. Rozpr. Monogr. UG, Gdańsk, 103 pp. (in Polish).

Pimenov, N.V., Ulyanova, M.O., Kanapatsky, T.A., Veslopolova, E.F., Sigalevich, P.A., Sivkov, V.V., 2010. *Microbially mediated methane and sulfur cycling in pockmark sediments of the Gdansk Basin, Baltic Sea*. Geo-Mar. Lett. 30, 439–448. https://doi.org/10.1007/s00367-010-0200-4

Pizzetti, I., Lupini, G., Bernardi Aubry, F., Acri, F., Fuchs, B.M., Fazi, S., 2016. *Influence of the Po River runoff on the bacterioplankton community along trophic and salinity gradients in the Northern Adriatic Sea*. Mar. Ecol. 37, 1386–1397.

https://doi.org/10.1111/maec.12355

Poulton, S., Canfield, D., 2005. *Development of a sequential extraction procedure for iron: Implications for iron partitioning in continentally derived particulates*. Chem. Geol. 214, 209–221. https://doi.org/10.1016/j.chemgeo.2004.09.003

Purkamo, L., Ehlert von Ahn, C.M., Jilbert, T., Muniruzzaman, M., Bange, H.W., Jenner, A.-K., Böttcher, M.E., Virtasalo, J.J, 2022. *Impact of submarine groundwater discharge on biogeochemistry and microbial communities in pockmarks*. Geochim. Cosmochim. Acta 334, 14–44. https://doi.org/10.1016/j.gca.2022.06.040

Quast, C., Pruesse, E., Yilmaz, P., Gerken, J., Schweer, T., Yarza, P., Peplies, J., Glöckner, F.O., 2013. *The SILVA ribosomal RNA gene database project: improved data processing and web-based tools*. Nucleic Acids Res. 41, D590–D596. https://doi.org/10.1093/nar/gks1219

Quinn, T.P., Erb, I., Gloor, G., Notredame, C., Richardson, M.F., Crowley, T.M., 2019. *A field guide for the compositional analysis of any-omics data*. GigaScience 8, giz107. https://doi.org/10.1093/gigascience/giz107

R Core Team, 2022. *R: A Language and Environment for Statistical Computing*. R Foundation for Statistical Computing, Vienna, Austria.

Riedinger, N., Formolo, M.J., Lyons, T.W., Henkel, S., Beck, A., Kasten, S., 2014. *An inorganic geochemical argument for coupled anaerobic oxidation of methane and iron reduction in marine sediments*. Geobiology 12 (2), 172–181. https://doi.org/10.1111/gbi.12077

Raiswell, R., Canfield, D.E., 2012. *The iron biogeochemical cycle past and present*. Geochem. Perspect. 1, 1–220. https://doi.org/10.7185/geochempersp.1.1

Rozan, T.F., Taillefert, M., Trouwborst, R.E., Glazer, B.T., Ma, S., Herszage, J., Valdes, L.M., Price, K.S., Luther, G.W. III, 2002. *Iron-sulfur-phosphorus cycling in the sediments of a shallow coastal bay: implications for sediment nutrient release and benthic macroalgal blooms*. Limnol. Oceanogr. 47, 1346–1354. https://doi.org/10.4319/lo.2002.47.5.1346

Ruff, S.E., Biddle, J.F., Teske, A.P., Knittel, K., Boetius, A., Ramette, A., 2015. *Global dispersion and local diversification of the methane seep microbiome*. Proc. Natl. Acad. Sci. U.S.A. 112, 4015–4020. https://doi.org/10.1073/pnas.14218651

Runge, E., Mansor, M., Chiu, T.H., Shuster, J., Fischer, S., Kappler, A., Duda, J.P., 2024. *Hydrothermal sulfidation of biogenic magnetite produces framboid-like pyrite*. Commun. Earth Environ. 5, 252. https://doi.org/10.1038/s43247-024-01400-z

Sánchez-Román, M., McKenzie, J.A., Wagener, A.L.R., Rivadeneyra, M.A., Vasconcelos, C., 2009. *Presence of sulfate does not inhibit low-temperature dolomite precipitation*. Earth Planet. Sci. Let. 285, 131–139. https://doi.org/10.1016/j.epsl.2009.06.003

Scanlon, K.M., Knebel, H.J., 1989. *Pockmarks in the floor of Penobscot Bay, Maine*. Geo-Mar. Lett. 9, 53–58. https://doi.org/10.1007/BF02262818

Schrum, H.N., Murray, R.W., Gribsholt, B., 2012. *Comparison of Rhizon sampling and whole round squeezing for marine sediment porewater*. Sci. Dril. 13, 47–50. https://doi.org/10.2204/iodp.sd.13.08.2011

Sivan, O., Adler, M., Pearson, A., Gelman, F., Bar-Or, I., John, S.G., Eckert, W., 2011. *Geochemical evidence for iron-mediated anaerobic oxidation of methane*. Limnol. Oceanogr. 56, 1536–1544. https://doi.org/10.4319/lo.2011.56.4.1536

Söderberg, P., Flodén, T., 1997. *Stratabound submarine terraces and pockmarks – indicators of spring sapping in glacial clay, Stockholm Archipelago, Sweden*. [In:] Cato, I., Klingberg, F. (Eds.), *Proceedings of the Fourth Marine Geological Conference – The Baltic, Uppsala*, pp. 1995.

Suess, E., 1979. *Mineral phases formed in anoxic sediments by microbial decomposition of organic matter*. Geochim. Cosmochim. Acta 43, 339–352. https://doi.org/10.1016/0016-7037(79)90199-6

Sundby, B., Anderson, L.G., Hall, P.O.J., Iverfeldt, A., Rutgers van der Loeff, M., Westerlund, S., 1986. *The effect of oxygen on release and uptake of cobalt, manganese, iron and phosphate at the sediment-water interface*. Geochim. Cosmochim. Acta 50, 1281–1288. https://doi.org/10.1016/0016-7037(86)90411-4

Szymczycha, B., Böttcher, M.E., Ehlert von Ahn, C.M., Diak, M., Koziorowska-Makuch, K., Kuliński, K., Makuch, P., Winogradow, A., 2023. *The benthic-pelagic coupling affects the surface water carbonate system above groundwater-charged coastal sediments*. Front. Mar. Sci. 10, 1218245. https://doi.org/10.3389/fmars.2023.1218245

Teichert, B.M.A., Bohrmann, G., Suess, E., 2005. *Chemoherms on Hydrate Ridge – Unique microbially-mediated carbonate build-ups growing into the water column*. Palaeogeogr. Palaeoclimatol. Palaeoecol. 227, 67–85. https://doi.org/10.1016/j.palaeo.2005.04.029

Thang, N.M., Bruchert, V., Formolo, M., Wegener, G., Ginters, L., Jørgensen, B.B., Ferdelman, T.G., 2013. *The impact of sediment and carbon fluxes on the biogeochemistry of methane and sulfur in littoral Baltic Sea sediments (Himmerfjärden, Sweden)*. Estuar. Coast. 36, 98–115. https://doi.org/10.1007/s12237-012-9557-0

Thiel, J., Byrne, J.A., Kappler, A., Schink, B., Pester, M., 2019. *Pyrite formation from FeS and H2S is mediated through microbial redox activity*. PNAS 116, 6897–6902. https://doi.org/10.1073/pnas.1814412116

Uścinowicz, S., Kramarska, R., Miotk-Szpiganowicz, G., 2011. *Geological setting and bottom sediments in the Baltic Sea*. [In:] Uścinowicz, S. (Ed.), *Geochemistry of Baltic*

Sea Surface Sediments. Polish Geological Institute – National Research Institute, Warsaw, 66–82.

Virtasalo, J.J., Schröder, J.F., Luoma, S., Majaniemi, J., Mursu, J., Scholten, J., 2019. *Submarine groundwater discharge site in the First Salpausselkä ice-marginal formation, south Finland*. Solid Earth 10, 405–423. https://doi.org/10.5194/se-10-405-2019

Vasconcelos, C., McKenzie, J.A., Warthmann, R., Bernasconi, S.M., 2005. *Calibration of the σ18O paleothermometer for dolomite precipitated in microbial cultures and natural environments*. Geology 33, 317–320. https://doi.org/10.1130/G20992.1